Three-way Catalysis with bimetallic supported Pd-Au catalysts:

Gold as a poison and as a promotor

Viktor Ulrich, Boris Moroz[1,2], Pavel Pyrjaev[1], Ilya Sinev[3],
Andrey Bukhtiyarov[1], Evgeny Gerasimov[1,2],
Valerii Bukhtiyarov[1,2], Beatriz Roldan Cuenya[3,4],
and Wolfgang Grünert*

Lehrstuhl Technische Chemie, Ruhr-Universität Bochum,
D-44780 Bochum, Germany

[1] Boreskov Institute of Catalysis, Novosibirsk 630090, Russian Federation
[2] Novosibirsk State University, Novosibirsk 630090, Russian Federation
[3]Department of Physics, Ruhr-Universität Bochum, D-44780 Bochum, Germany
[4] Department of Interface Science, Fritz-Haber-Institut der Max-Planck-Gesellschaft, D-14195 Berlin, Germany

In memoriam Prof. Maria Flytzani-Stephanopoulos

*Corresponding Author:

Prof. W. Grünert, Lehrstuhl Technische Chemie, Ruhr-Universität Bochum, P. O. Box 102148, D-44780 Bochum, Germany, Tel. +49 234 322 2088, Fax +49 234 321 4115,

email w.gruenert@techem.ruhr-uni-bochum.de

Keywords: Ageing; support influence, alloying; XRD; XANES

Abstract

Three-way catalysts containing Au and/or Pd supported on either $CeZrO_x$ (CZ) or La_2O_3/Al_2O_3 (LA) were studied with respect to their performance in a model feed and characterized by various techniques (physisorption, CO chemisorption, TEM, XRD, XPS, XANES). A drastic support influence was found in both catalytic behavior and Pd-Au relation. While Au was a strong poison for all catalytic functions of Pd (oxidation, NO reduction) on LA, poisoning was much mitigated on CZ, rendering all Pd containing catalysts superior to a commercial reference. After ageing, the poisoning by Au was aggravated on LA. On CZ, Pd-rich bimetallic combinations retained better activity than Pd/CZ, which still outperformed the reference. As Au did not significantly contribute to propene oxidation and NO reduction, activity of Pd was markedly increased under a promoting influence of Au. Stabilization of Pd^{II} by ceria and delayed Pd-Au alloy formation are key features in the CZ-supported PdAu catalysts.

1. Introduction

Three-way catalysis, which converts the harmful exhaust components CO, unburned hydrocarbons (HC), and NO_x (NO and NO_2) into CO_2, N_2, and H_2O, is a cornerstone of the technology for mitigating the environmental impact of cars. It remains, therefore, an important area of research and innovation [1]. In traditional three-way catalysts (TWCs), the active components Pt, Pd, and Rh are supported in different combinations on refractive oxides as γ-Al_2O_3 and ZrO_2, which are stabilized against sintering by additives (e.g., BaO, La_2O_3), or on the oxygen storage component, which is typically based on Ce-Zr mixed oxides [2]. Low-temperature operation, e.g. during the cold start phase or under idling conditions, belongs to the challenges even with the mature catalyst formulations available nowadays. While it can be addressed by a number of secondary approaches (traps, close-coupled converters) [3], further improvement of the TWC itself might solve the problem more directly.

In the effort to enhance the low-temperature performance of TWCs, the attention to nanoparticulate gold, which combines an extraordinary activity for CO oxidation [4] with appreciable activity for hydrocarbon oxidation [5] and even for the selective reduction of NO by propene [6], was limited so far. This may have been due to the low melting point of the metal, although several groups have reported that the thermal stability of gold nanoparticles on the surface of Al_2O_3 and some other oxides by far exceeds expectations based on melting behavior due to a quasi-epitaxial interaction between small Au crystallites and the support surface [7-12]. In an early study of Mellor et al. [13], which was later discussed by several authors without new evidence [14-16], Au deposited on a complex support was shown to catalyze all required reactions under reducing conditions, although the light-off temperature (T_{50} - temperature of 50 % conversion) was rather high for NO reduction: ≈573 K for a sample additionally containing Rh, 653 K without Rh. Under oxidizing conditions, NO reduction did not reach even 50 % conversion [13].

In a recent study, our group confirmed the attractive oxidation activity of monometallic Au on several supports. Gold outperformed a commercial reference catalyst in particular when supported on $CeZrO_x$, while the NO reduction conversion hardly ever achieved 40 % even under stoichiometric conditions [17]. However, in the model feed containing CO, propene, and NO, a strong inhibition of CO oxidation by propene was observed, which was most persistent under dry conditions and on irreducible supports (γ-Al_2O_3, La-Al_2O_3), while the increase of T_{50} found for $Au/CeZrO_x$ was only moderate. In a subsequent study on reactant interactions in three-way catalysis over supported gold catalysts [18], we identified two poisoning mechanisms, one of them based on competitive adsorption combined with unfavorable electron transfer. The other one operating at somewhat higher temperatures in propene-containing feed, was ascribed to the deposition of carbonaceous residues around the Au particles. These residues, which did not block CO adsorption sites, but prevented the supply of active oxygen by the adjacent support surface, were combusted by the active oxygen upon temperature increase. As a result, poisoning was lifted under conditions which depended on the availability of active oxygen species on the support surface.

With respect to durability, the oxidation activity of supported Au catalysts was only moderately affected by a 6 h exposure to an atmosphere containing 5 % O_2 and 10 % H_2O at 923 K, well in agreement with earlier reports on surprising thermal stability of Au nanoparticles [7-12]. An analogous treatment at 1223 K caused, however, inacceptable, though not complete, deactivation [17].

In the light of these results, we have now examined the combination of Au with a different noble metal in order to improve its behavior with regard to two aspects: to delay sintering by anchoring it at the surface of a more refractory metal, and to combat coking of the adjacent support surface by using a metal active for the hydrocarbon oxidation. A similar approach was proposed by some of us earlier for the application of Au in diesel oxidation, where physical mixing of Au and Pt-based catalysts protected gold from deactivation by hydrocarbons [19].

Among the noble metals relevant for TWC, Pd was selected, because it can be easily differentiated from Au in diffraction and X-ray absorption techniques. With Pd prices currently exceeding those of gold, this choice has meanwhile acquired even practical relevance. Among the supports used in [17] and [18], γ-Al_2O_3 and $CeZrO_x$ exerted the most divergent influences on the supported Au particles. However, given its importance in real three-way catalysis, La-Al_2O_3 was compared with $CeZrO_x$ in the present study instead of γ-Al_2O_3.

Much attention has been paid to supported PdAu catalysts in recent literature because of their attractive catalytic properties in a number of reactions, e.g. vinyl acetate synthesis [20], CO oxidation [21-31], total oxidation of hydrocarbons [32, 33], anodic oxidation of H_2 [34], H_2O_2 synthesis [35], N_2O decomposition [36], reduction of NO by CO [37], in the selective oxidation of alcohols [38], of toluene [39], and of styrene [40]. Their application in a model lean engine effluent (CO, propene, NO, with excess oxygen) was described in recent patents (e.g. [41]), where full conversion was reported for CO at 423 K and for propene at 450 K, while the fate of NO was not commented. In open literature, there is ample coverage of CO oxidation, mostly, however, in excess oxygen, and some studies on total hydrocarbon oxidation and on NO reduction with CO.

With respect to CO oxidation, results of theoretical calculations and studies on model catalysts raise the expectation that the activity of Pd can be improved by alloying with Au, although Pd-rich compositions may be unfavorable [21, 42, 43]. Literature reports on CO oxidation with real supported bimetallic catalysts are inconsistent, but mostly in conflict with these predictions. PdAu supported on the weakly interacting SiO_2 support should be most similar to the model systems. However, several studies with SiO_2-supported PdAu catalysts agree in the deleterious influence of Au on the CO oxidation activity of Pd/SiO_2 [22-24]. While some groups reported even monometallic Au to be inferior to Pd on the SiO_2 support [22, 23], Qian et al. [24] found Au/SiO_2 to convert CO at lower temperature than Pd/SiO_2, but with a unusual temperature dependence featuring a peak conversion <100 % instead of the well-known S-shaped conversion

curve, which was exhibited by Pd/SiO_2. The mechanism operating on Au/SiO_2 was poisoned by adding Pd and the mechanism operating on Pd/SiO_2 was poisoned by adding Au, i.e. catalysts with intermediate metal ratio were inefficient in both mechanisms and exhibited deplorable performance. Opposed to this, Xu et al [25] found small amounts of Au causing enormous improvement over monometallic Pd/SiO_2, though not beyond the activity of monometallic Au/SiO_2 (with an S-shaped conversion curve), while Au-rich alloys lagged even behind monometallic Pd.

In a study comparing alumina- and titania-supported Au-rich AuPd alloys for CO oxidation and cyclohexene hydrogenation, Ward et al. [26] found the alloys somewhat less active than Au on Al_2O_3, but somewhat more active on TiO_2, while CO oxidation could not be detected at all over the monometallic Pd catalysts under the respective conditions. From work with alumina-supported PdAu, Suo et al. [27] derived that the alloyed surface provides low activity while coexistence of PdO with Au is favorable. In a remarkable contradiction to the data in ref. [26], Guczi et al. reported comparable values for both reaction rate and TEM-related TOF for Au/TiO_2 and Pd/TiO_2 while the rate over a bimetallic catalyst slightly exceeded the value expected by linear combination of Pd and Au contributions [28]. In later work of the same group [29], the Pd/TiO_2 reference was even superior to Au/TiO_2 while no synergism was observed in the alloy catalysts studied.

Comparing the catalytic behavior of supported PdAu alloys in gas- and liquid-phase reactions, Carter et al. [30] used a similar Ce-Zr oxide support as in the present study. The response of CO oxidation to alloying reminded that reported by Qian et al [24] for SiO_2-supported alloys: Pd poisoned Au gradually, rendering Au_1Pd_1 still more active than monometallic Pd, and Au poisoned Pd. As a consequence, the lowest activities were obtained with Pd-rich compositions. Covering only Au/Pd ratios ≥1, Olmos et al. [31] observed a similar monotonous decrease of activity when Pd was added to $CeZrO_x$-supported gold, with Au_1Pd_1/ $CeZrO_x$ still slightly exceeding the monometallic $Pd/CeZrO_x$. Different from observations of Qian et al. with the

silica support [24], gold oxidized CO along the typical S-shaped temperature dependence of conversions when supported on $CeZrO_x$ [31].

Unlike CO oxidation, coverage of hydrocarbon oxidation and NO reduction is scarce in the literature. However, the optimistic outlook of ref. [21] on the oxidation activity of PdAu catalysts was supported by a study of propene and toluene combustion over PdAu supported on mesoporous TiO_2 [33], where light-off temperatures between 470 and 530 K were obtained for different bimetallic samples, more than 100 K below T_{50} of Au/TiO_2. A core(Au)-shell(Pd) preparation and an alloyed catalyst even outperformed the Pd/TiO_2 reference. In work with an AuPd(100) model catalyst, Gao et al. [44] found enhanced activity in NO reduction by CO and improved N_2 selectivity compared to the unmodified Pd(100) surface: these authors even recommended combining Pd with gold for solving the cold-start problem.

Thus, while the literature suggests a loss in CO oxidation activity upon alloying gold with Pd, a moderate decrease may be an acceptable price for an improvement in both NO reduction and hydrocarbon oxidation activity.

The present paper is focused on the catalytic data of the bimetallic catalysts in a TWC model feed, which highlight drastic differences in the performance of the PdAu combination on two supports (La-Al_2O_3, $CeZrO_x$) and a benefit of adding gold much different from the expectations. In this paper, information on structural properties will be confined to the results of standard characterization of the initial catalysts and some key experiments that shed light on the likely reasons of the differences in performance. A more detailed analysis of the interactions between Pd, Au, and the support surfaces in the initial state and after relevant thermal treatments will follow in a subsequent publication.

2. Experimental

2.1. Catalyst preparation

Pd and/or Au were deposited on supports that were already used in our earlier work [17, 18]: La-stabilized Al_2O_3 containing ca. 2 wt-% La, (further abbreviated by LA, donated by Sasol Germany GmbH) and ceria-zirconia mixed oxide ("CZ"), donated by Umicore & Co. KG Hanau (Germany). The bimetallic catalysts were prepared in a two-step protocol along the direct redox route described in refs. [45] and [46].

Pd was initially introduced by incipient wetness impregnation using a solution of $Pd(NO_3)_2$ in 0.15 M HNO_3. After drying in air overnight, the samples were heated in flowing Ar at 393 K for 2 h and at 523 K for another 3 h. The Pd was reduced in flowing H_2 during a 3 K/min temperature ramp from 393 to 523 K and a 2 h isothermal hold at 523 K, followed by cooling to room temperature in H_2. For the introduction of Au, the atmosphere was changed to Ar and the samples were transferred under inert conditions to a thermostated glass reactor, in which an aqueous Au solution obtained by neutralization of $HAuCl_4$ with NaOH and purged with Ar was added to the freshly reduced Pd-containing samples (deposition-precipitation technique [47, 48]. The suspension was quickly heated to 343 K and kept at this temperature under vigorous shaking. After filtration, washing with water, and drying in vacuo at 333 K, the samples were finally reduced in flowing hydrogen at 523 K for 2 h. The preparation of monometallic Au catalysts was reported in ref. [17].

For reference, the catalytic behavior of a commercial TWC donated by Interkat Katalysatoren GmbH (Königswinter, Germany, Pd : Pt : Rh = 13 : 1 : 1, total precious metal content ≈2 wt.%) was also studied.

2.2. Catalyst Characterization

The catalysts were characterized in their initial states and after a thermal ageing procedure (see section 2.3) by a number of techniques.

Precious metal contents were determined by X-ray fluorescence analysis using an ARL instrument (Rh anode, operated at 50 kV, 40 mA). The support texture was studied in both states by

nitrogen physisorption at 77 K after previous outgassing at 673 K using a Quantachrome Autosorb-1-MP instrument. The surface area was evaluated from the isotherms applying the BET equation to the p/p_0 = 0.05 - 0.35 range, the pore volume was determined at p/p_0 = 0.98, and the mean pore size was obtained from a standard BJH treatment of the data.

The Pd dispersion $f_{Pd} = n(exposed)/n(total)$ in the initial samples was determined by CO chemisorption by exposing the samples to CO pulses in flowing He at 294 K. The method has been described in some detail in [49]. Prior to the measurement, the samples were treated in flowing H_2 at 373 K for 15 min, with subsequent cooling in hydrogen. For the evaluation of *n(exposed)*, a stoichiometry of CO/Pd = 1 was assumed. Reproducibility was ±1.5 $\%_{rel}$ or better. We are aware that the real stoichiometric coefficient should be between 0.7 and 1 because of the existence of bridged forms of adsorption. On mixed AuPd surfaces, this stoichiometry is, however, likely to vary in this range. As our intention was to identify pronounced tendencies rather than to evaluate exact particle sizes, CO/Pd = 1 should be an acceptable approximation. Monometallic Au did not adsorb CO under the conditions of the pulse technique.

Electron micrographs of the initial samples were obtained with a JEM-2010 instrument (JEOL, Japan) at an acceleration voltage of 200 keV, where lattice resolution is specified as 0.14 nm. Particle size analysis was performed sampling between 180 and 320 particles, assuming a spherical particle shape.

X-ray diffractograms of samples after preparation and after thermal ageing were recorded in a range of 2Θ = 5-90 ° with an Panalytical Empyrean diffractometer using CuKα radiation (λ = 1.540598 Å). Crystalline phases were identified by employing the powder diffraction files (PDF) of the International Center of Diffraction Data (ICDD) and the X'Pert HighScore Plus software (Panalytical).

X-ray photoelectron spectra of the initial samples were measured on a SPECS instrument equipped with a Phoibos-150-MCD-9 hemispherical analyzer, using non-monochromated MgKα radiation (hν =1253.6 eV, 150 W). The charging effect was corrected using the Zr 3d

peak from CZ at 182.3 eV or the Al 2p peak from LA at 74.5 eV as an internal reference. Line intensities were integrated over Shirley backgrounds, and the atomic concentrations were evaluated from them using Scofield atomic sensitivity factors [50].

X-ray absorption spectra at the AuL_{III} and Pd*K* edges (11.919 and 24.350 keV, respectively) were measured at station P65 of the Petra III storage ring (Hasylab at Desy, Hamburg, Germany). Supplementary measurements were performed at the CLAESS beamline at Alba (Barcelona, Spain) and at the BioXAS beamline at the Canadian Light Source (CLS, Saskatoon, Canada). The spectra shown in this paper refer to the state of the catalysts after preparation (with a final reduction at 523 K) and after ageing at 1223 K (see section 2.3). After the treatments, the samples were cooled to room temperature in He, pressed to pellets of suitable optical path lengths and wrapped in Kapton. During this conditioning, the exposure to ambient was less than 2 h. The spectra were recorded at room temperature. All scans were repeated on the same sample to ensure reproducibility.

In the present paper, the XAS analysis will be limited to the XANES region, the EXAFS will be discussed in a subsequent paper. Data treatment was carried out with the software package ATHENA [51]. It comprised adjustment of the energy scale, subtraction of the pre-edge background with a Victoreen polynomial fitted to the pre-edge region, and normalization to the step height. From the Pd*K*-edge XANES, the abundance of Pd in the oxidation states 0 and +2 was estimated by Linear Combination Fitting (LCF) using the XANES of the Pd/LA sample after ageing at 1223 K and of PdO as references.

2.3. Catalytic studies

The catalytic behavior was studied in a microflow reactor at atmospheric pressure ramping the temperature between 323 and 673 K or 823 K at 5 K/min as described in more detail elsewhere [17]. 183 mL min^{-1} of a stoichiometric model feed consisting of 1.1 vol-% CO, 0.1 vol-% NO, 0.1 vol-% propene, 0.95 vol-% O_2, and 10 vol-% H_2O, balance He were fed over 125 mg of

quartz-diluted catalyst samples, which resulted in a gas-hourly space velocity (GHSV) of 60,000 h^{-1}. After removing moisture from the effluent stream by a cold trap, the effluent components were analyzed by combining calibrated mass spectrometry (O_2, NO, propene) and non-dispersive IR photometry (CO, CO_2, N_2O), with due account of the N_2O fragmentation pattern on mass-spectrometric NO analysis. Conversions were evaluated using eq. (1) (given for CO, index 0 – initial)

$$X_{CO} = \left(c_{0,CO} - c_{CO}\right)/c_{0,CO} \qquad (1)$$

N_2O formation will be reported as ppm content in the effluent.

Catalytic data will be also reported for the state achieved after using the catalysts for a certain period of time (stabilized state). The data were measured in a fourth temperature ramp from room temperature to 670 K following three ramps with successive feed variation (stoichiometric, rich, lean). To examine durability, the catalysts were calcined in a flow of 5 % O_2 and 10 % H_2O, balance He, at the same GHSV for 6 h at 923 K or at 1223 K. The presentation will be focused on the results obtained after the latter treatment.

3. Results and Discussion

3.1 Structural properties of supported PdAu catalysts

3.1.1 Composition, texture, particle size from electron microscopy and CO chemisorption

Precious metal contents of the samples are reported in Table 1 together with the labels used in this paper for their identification. In the preparations, a noble metal content of 2 wt-% was targeted. The results of chemical analysis show that this was successful. A few outliers (Au/CZ, Au_4Pd/CZ) deviate by just 20 %, which is insufficient to explain the drastic differences in the catalytic behavior to be described below. The bimetallic catalysts were designed to have a Pd-rich, an Au-rich and a 1 : 1 composition. This was achieved as well. For the CZ support, data from a catalyst with a moderate Pd excess ($AuPd_2$) will be also reported.

Examples for micrographs used for the determination of average metal particle sizes are shown in the supporting information together with histograms of the particle size distribution (Figures S1, S2). Micrographs of the monometallic Au catalysts were shown in [17]. In the resolution achieved, it is not possible to decide if the metals are mixed or segregated in the nanoparticles. Number-weighted average sizes of metal particles (d_l) are summarized in Table 1 (for volume/surface- and mass-weighted averages see Figures S1 and S2). They are mostly well below 3.5 nm. On the LA support, they are scattered between 1.6 and 3.2 nm. Overlap between ranges covered by the standard deviations around almost all d_l values discourages the identification of tendencies. The range of particle sizes is much wider on the CZ support, where standard deviations are quite small in some cases. A rather distinct tendency to smaller particles in Pd-rich compositions is disrupted by $AuPd_4$. It is, however, worth noting that the particle size of monometallic Pd is significantly below the Au particle size on CZ while it is comparable on LA, maybe even slightly larger.

Table 1 reports also evidence on the accessibility of Pd atoms as measured by CO chemisorption. The Pd dispersion is ≈0.3 on the LA support, but clearly larger, mostly around 0.5 on CZ. It will be shown below that Pd was partly ionic in the initial catalysts, on CZ to a larger extent than on LA. Corrected Pd dispersions were evaluated by relating the CO chemisorption capacity only to Pd^0, the percentage of which was estimated from the XANES (see Table 4 below). The dispersion is slightly above 1 for the CZ-supported samples, which suggests that all Pd^0 atoms in them were accessible from the gas phase. The complete accessibility of Pd^0 is well in agreement with particle sizes of 1 nm (Table 1) where deviations from the spherical shape due to interactions with the support are likely anyway, but it disagrees with particle sizes of 3 nm as found in most Au-containing samples. It may be therefore assumed that the larger particles contain almost no Pd, while Pd^0 coexists with these gold particles decorating them or (contrary to intentions) segregated in separate patches. It is unclear why gold was not deposited in larger particles in $AuPd_2$/CZ. For the LA-supported catalysts,

the corrected dispersions were in the range of 0.4-0.6. These values are compatible with the particle sizes reported.

Typical texture data of our catalysts are summarized in Table 2. It can be seen that the introduction of two metals via two wet procedures slightly decreased the BET surface area, in the case of LA also the mean pore diameter. The variation of the metal ratio had little influence on the texture, with the exception of a moderate drop in the BET surface area of $AuPd_4$/CZ. As expected, ageing at 1223 K significantly decreased the BET surface area of both supports, with the stronger decrease for CZ. Notably, the pore volume of LA was not affected at all by the thermal stress – it just became accommodated in wider pores. The increase of pore widths was less pronounced in CZ, therefore, the support had lost much of its pore volume after treatment at 1223 K.

3.1.2 X-ray Diffraction

In Figure 1, relevant parts of the X-ray diffractograms of all catalysts in the initial state (i.e. after a final reduction at 523 K, cf. section 2.1.) are presented. The 2Θ regions were selected to allow observing reflections of Au and Pd undisturbed from the support reflections, which is illustrated by some examples for full-range diffractograms presented in Figure S3. In the case of CZ (Fig. 1a), this is possible between 35° and 48° where the (111) and (200) reflections appear at 38.18° (Au) and 40.12° (Pd) and at 44.39 ° (Au) and 46.66 ° (Pd), respectively. In the diffractograms of LA-supported samples, the support exhibits intense signals in this range, but also beyond, none of the Au(Pd) reflection appears without any overlap with the support. Fig. 1b shows the 70 – 90 ° range allowing the best tradeoff between a broad and weak Al_2O_3 signal at 77.22° and the 311 reflections of Au (77.55°) and Pd (82.10°), while even the (222) reflection (for Au expected at 81.72 °, for Pd at 86.22°) could be observed in some samples.

The most conspicuous feature observed with the CZ-supported catalysts is that all Au-containing samples exhibit an Au reflection while there is hardly any indication of Pd even in the

diffractogram of the monometallic Pd/CZ (Fig. 1a). The inclined background feigns an asymmetry of the Au(111) reflection as illustrated by the Au/CZ sample. The behavior of this signal with increasing Pd content is complex: while there is hardly any shift on the angle that might indicate alloying, the signal becomes narrower and very small at higher Pd content. From the line width of Au/CZ (1.34°), an average crystallite size of 6.1 nm can be deduced with the Scherrer equation, about twice the mass-weighted size observed in the TEM (Fig. S2). The apparent contradiction between the TEM and XRD data on the particle sizes (see also below) can be explained by the fact that the samples contain coarse Au crystallites, which could be seen only in a few micrographs. Some examples are shown in Figure S4, the situation is similar as encountered in earlier work [52]. As these aggregates are irrelevant for catalysis, they have not been in the particle size distribution. With increasing Pd content, the line width decreases to 0.33° ($AuPd_2$/CZ), and slightly increases again to 0.53° in $AuPd_4$/CZ, which corresponds to crystallite sizes well beyond 15 nm. At the same time, there is no change of the signal width at the base from Au/CZ to AuPd/CZ, which indicates the coexistence of smaller particles. Indeed, the Au(111) reflection of AuPd/CZ is clearly composed of a narrow and a broad signal, indicating a bimodal particle size distribution as has been observed earlier and supported by Rietveld analysis in Au/C and AuPd/C preparations in refs. [53, 54] At higher Pd content, the (111) signal becomes narrow also at the base: the smaller particles fall below the detection limit of XRD in these samples. Indeed, relative to Au/CZ, the area of the (111) reflection in $AuPd_2$/CZ and $AuPd_4$/CZ decreased stronger (by 75 % and 80 %, respectively) than the Au content (by 38 and 56 %, respectively, cf. Table 1). The shape of the superimposed broad (111) reflection of AuPd/CZ suggests, that they contain only a small percentage of Pd, if any, but there is no evidence on that point for the Pd-rich samples.

On the LA support (Fig. 1b), the relation between Au and Pd is very different. The series on the two supports resemble only in the poor visibility of the Pd signal in the monometallic catalyst.

As in Pd/CZ, an intensity assignable to Pd^0 can be discerned only by subtracting the diffractogram of the support from that of Pd/LA. On the other hand, already in Au_3Pd/LA, the Au(311) reflection is slightly shifted towards higher 2Θ relative to the very broad (311) signal in Au/LA. In AuPd/LA, the alloying is quite obvious, but the signal is decreased. In $AuPd_4$/LA, a (311) signal can be discerned only by subtracting the support background, and its 2Θ indicates a Pd-rich composition. The decreasing signal intensities suggest a very high dispersion of the alloy particles, but a coexistence of alloyed and monometallic Pd clusters cannot be excluded.

Diffractograms taken after ageing at 1223 K (Figure 2) reveal a number of processes induced by the thermal stress. The much narrower line widths are according to expectations. On the monometallic Au catalysts, the average crystallite size has increased to ca. 10 nm on LA, and 20 nm on CZ. But now, the monometallic Pd catalysts exhibit intense and narrow lines as well, which indicate similar particle sizes. Alloys have been formed in all bimetallic catalysts, but with characteristic differences. On CZ, the average compositions derived from the peak position via the Vegard rule, are significantly enriched in Au: $Au_{6.5}Pd$ in Au_4Pd/CZ, Au_4Pd in AuPd/CZ, and AuPd in $AuPd_4$/CZ. These (111) reflections are much broader than those of the monometallic catalysts. This is, however, most likely not due to a small particle size, but rather to a distribution in the composition of particles, as illustrated also by the shape of the (200) reflections at $2\Theta \approx 45°$. Notably, CZ-supported catalysts with an Au/Pd metal ratio ≤1 contain non-alloyed Pd coexisting with the alloy particles, which supports the assumption of non-alloyed Pd patches in the initial catalysts made on the basis of CO chemisorption data. On the contrary, non-alloyed gold is not present to any significant extent at Au/Pd ≥ 1, where bimodal particle size distributions were identified in the initial samples. Apparently, on the CZ surface, even the large Au particles of the initial samples were included in alloying with Pd during the thermal treatment.

As already in the initial samples (Fig. 1b), the tendency of alloying is more pronounced on the LA than on the CZ support (Fig. 2). In AuPd/LA, the average alloy composition is near the nominal one ($Au_{1.05}Pd$, cf. Table 1, $Au_{1.25}Pd$ from Fig. 2b). The samples with one excess component contain a wide distribution of alloy compositions around the nominal ones: Au_3Pd/LA from $Au_{13}Pd$ to $Au_{2.3}Pd$, $AuPd_4$/LA from $AuPd_{1.6}$ to Au_0Pd (Fig. 2b). The tendency to preserve non-alloyed Pd particles is higher on CZ than on LA. Segregated Pd exists in AuPd/CZ (where the Au/Pd ratio is actually 1.5, cf. Table 1), but not in AuPd/LA. At Pd excess, there is a wide continuum of alloy compositions (though with peaks at $AuPd_{1.6}$ and at pure Pd) on LA (Fig. 2b) while the abundance of particles with intermediate compositions between Au/Pd ≈ 1 and pure Pd is very small on CZ (Fig. 2a).

3.1.3. XPS

Photoelectron spectra measured with the bimetallic supported AuPd catalysts in the initial state are reported in Figures S5 and S6, the most important results are summarized in Table 3. The Pd 3d region is overlapped by the Au $4d_{5/2}$ peak. The Pd 3d spectra of LA-supported Au-Pd catalysts shown in Fig. S5 were obtained by subtraction of the Au $4d_{5/2}$ contribution deduced from the shape and the area of the (non-affected) Au $4d_{3/2}$ component from the experimental signal. Unfortunately, on the CZ support, this binding energy (BE) region is additionally overlapped by the intense Zr 3p doublet of the CZ support. Therefore, no quantitative data could be extracted for CZ-supported palladium. The gold is metallic in all cases, while a significant part of the Pd was found in the +2 oxidation state on the LA support. Some shoulders at the intense Zr 3p signals (Figure S6) suggest that metallic and oxidized states of Pd may coexist also in the CZ-supported samples.

In the monometallic catalysts, the binding energies of Au and Pd are very close to those of the bulk metals. In LA-supported bimetallic catalysts, both Au $4f_{7/2}$ and Pd $3d_{5/2}$ (of Pd^0) are shifted to lower BEs by 0.3-0.4 eV, but without any trend. A significant, though smaller downshift can be also seen in Au $4f_{7/2}$ of the CZ-supported catalysts (Table 3). Such BE shifts have been often

claimed to indicate alloying [55-60]. However, due to the small effects and the complicated nature of samples and spectra, we are cautious with conclusions in the present case. The observed tendencies are not compatible with evidence from XRD: in the LA-supported catalysts, where some alloying is indeed confirmed by XRD, there is no trend on the BE shifts while there is one on the alloying degree (Figure 1b). A significant, though smaller shift was found also for Au in CZ-supported catalysts, while there does not seem to be any alloying in these samples (Fig. 1a, see; however, below).

As found in XPS work with the monometallic Au catalysts in [17], the concentration of Au (and likewise of Pd) in the near-surface region is close to the bulk concentration on the LA support (Table 3). This suggests that the particle size is mostly <2 nm, which is compatible with the evidence from TEM. On the other hand, Au is surface-enriched in the CZ-supported catalysts, most likely because of the lower surface area of CZ. Notably, the surface concentration of Au did not decrease with growing Pd content on the CZ support (Table 3). On LA, there was only a minor decrease of the surface Au concentration up to AuPd/LA. Conversely, the Pd surface concentration increased monotonously with growing Pd content. The resulting surface Au/Pd ratio was somewhat below the bulk one for Au_3Pd/LA ($(Au/Pd)_s$ = 1.9), while surface and nominal Au/Pd ratios were similar in the other catalysts.

3.1.4 X-ray Absorption: XANES

X-ray absorption spectra were measured for the catalysts used in this study in the initial state, for most samples after ageing at 1223 K (and after an analogous ageing at 923 K) and for selected samples after catalytic tests. In the present paper, the XANES in the initial state and after ageing at 1223 K are presented (for the AuL_{III}-edge in Figure S7, for the Pd*K*-edge in Figure 3) while the EXAFS will be discussed in a follow-up report dedicated to a more detailed study of the relation between Pd and Au.

Differences between the Au*L*$_{III}$-edge XANES of the initial CZ-supported catalysts are only minor (Fig. S7a). In the Au-rich catalysts, the weak structure in the XANEST of the Au foil is almost completely washed out, the peak at 11946 eV is slightly shifted to higher energies. This may be due to the small Au particle size in these catalysts. Conversely, the XANES of $AuPd_2$/CZ is very close to that of bulk Au, its structure is even more pronounced. The reason is not clear at the moment, but the presence of Au particles well above 10 nm as disclosed by XRD (Fig. 1a) may play a role for this effect. On the LA support, differences in the Au*L*$_{III}$ XANES spectrum are more pronounced (Fig. S7b). Compared with Au/CZ, Au/LA exhibits more intensity right above the edge, which may indicate some electron transfer from the gold to the support. Beyond the missing white line, the XANES of AuPd/LA and $AuPd_4$/LA differ also in a significant shift of the 11946 eV peak and a strong increase of the originally weak feature around 11935 eV.

Although the catalysts had been reduced at 523 K, the Pd *K*-edge XANES of the CZ-supported samples resembles more the XANES of PdO than that of bulk Pd (Fig. 3a). The less pronounced decrease towards 24390 eV in most spectra suggests, however, significant contributions also from the metal. On the LA support, the contribution of Pd^0, which results in a weak maximum around 24380 eV, is more visible (Fig. 3b). The distributions of Pd oxidation states obtained by LCF of the Pd*K*-edge XANES are presented in Table 4. It should be noted that some details of the XANES shapes, e.g. shoulders around 24373 eV in the XANES of Au_4Pd/CZ and $AuPd_2$/CZ (Fig. 3a), could not be resolved, but edge positions and shapes, white line intensities and the extent of the intensity decay towards 24390 eV were well reproduced. While the values in Table 4 are therefore subject to quite some uncertainty, the general trends revealed by them can be trusted.

The data shows that more than 50 % of the Pd atoms supported on CZ are in the cationic state – typically 50-70 %. On LA, Pd is not completely reduced either, but the percentage of oxidized Pd is lower – 35-45 %. Although Pd is partly oxidized on both supports, a significant percentage

of Pd is metallic. The almost complete absence of XRD intensity due to Pd in these catalysts can, therefore, not be ascribed exclusively to the oxidation of the metal. Rather, the Pd metal particles are extremely small on both supports.

After ageing at 1223 K, the Au*L*$_{III}$-edge XANES of CZ-supported samples (Fig. S7c) exhibits more changes than in the initial state (Fig. S7a), although the spectrum of AuPd/CZ is still almost identical with that of Au/CZ. At higher Pd contents, the spectra change in a similar way as observed with the initial LA-supported catalysts (Fig. S7b): the feature at 11946 eV shifts to higher energies and the intensity increases around 11935 eV, forming a weak maximum in AuPd$_4$/CZ. These tendencies are continued in the LA-supported catalysts (Fig. S7d), where the feature at 11935 eV develops into a pronounced second peak. The XANES of AuPd$_4$/CZ and AuPd$_4$/LA differ in the better definition of this signal and lower intensity in the white-line region of the latter. These changes obviously arise from interactions with palladium, most likely alloying (cf. Fig. 2b), which are more pronounced on the LA support.

These observations are corroborated by the Pd*K*-edge XANES spectra, which show Pd completely metallic on the LA support (Fig. 3d, see also Table 4). On CZ, (auto)reduction of Pd^{2+} can be also observed, but it is by no means complete: ca. 50 % of the Pd remains cationic – though with a remarkable exception (AuPd$_4$/CZ). It should be noted that the treatment temperature was well above the temperature of PdO decomposition (ca. 1020 K). This shows that Pd^{2+} is strongly stabilized by the surface of the Ce-containing oxide as has been reported earlier for cationic Pt [61] and later for Pd^{2+} by several groups [62-64].

3.2 Catalytic results

3.2.1 Initial catalysts

In Figures 4 and 5, the behavior of the CZ- and LA-supported mono- and bimetallic Au$_x$Pd$_y$ catalysts in the conversion of the TWC model feed is compared and contrasted with the performance of the commercial reference catalyst. In the CZ series (Fig. 4), the catalyst with

the Au/Pd metal ratio of 1 has been omitted to avoid overcrowding, the data can be found in the supporting information (Figure S8. The results show a major influence of the support on the catalytic properties.

All CZ-supported preparations of this study outperform the commercial reference in the oxidation reactions (Fig. 4a, b), the Pd-rich ones also in NO reduction (Fig. 4c). Moreover, the strong N_2O evolution of the reference catalyst in the light-off range was dramatically decreased over all catalysts of this study, although some of the catalysts released significant N_2O concentrations at lower temperatures. The positive first impression is, however, somewhat clouded by the observation that the best performance among all samples was delivered by the monometallic Pd/CZ. Although its advantage in CO oxidation (T_{50} = 375 K *vs*. 389-395 K for the other catalysts, see Fig. 4a; 385 K for AuPd/CZ, Fig. S8a) is apparently related to the enhanced low-temperature N_2O formation (Fig. 4d), Pd/CZ exhibited also the lowest light-off temperature for propene (Fig. 4b) and NO (Fig. 4c). The introduction of Au deteriorated the catalyst behavior, but not dramatically. Despite slight deficits around 50 % conversion, $AuPd_4$/CZ even stands out for the complete conversion of all components at temperatures where the other catalysts still approach 100 % rather gradually. This advantage was, however, lost already with $AuPd_2$/CZ. With increasing Au content, the light-off curves shifted to higher temperatures. The relation between CZ-supported Au_4Pd and Au may be noted as a remarkable detail. While the bimetallic catalyst achieved full NO conversion still at an acceptable light-off temperature and in great contrast to Au/CZ (Fig. 4c), it was outperformed by the monometallic sample in propene oxidation (Fig. 4b). AuPd/CZ fits completely into the ranking with respect to propene oxidation and NO reduction, although it behaved rather similar to Pd/CZ in CO oxidation (Fig. S8a). This low-temperature CO conversion was again accompanied by an enhanced N_2O release below 390 K.

The influence of stabilization on the catalytic behavior of the CZ-supported samples is reported in Figure S9, where the initial curves of Pd/CZ, $PdAu_2$/CZ, and Au/CZ are repeated for

comparison, and in Figure S10 for AuPd/CZ. After stabilization, the propene and NO conversion curves of all catalysts remained in narrow ranges and identical ranking, but were shifted upward by ca. 20 K. With only a few exceptions, the catalysts remained better than the (initial) reference catalyst (Fig. S9b, c). The effect of stabilization on CO oxidation was more severe (Fig. S9a): T_{50} of all catalysts were now in a ±7 K range around 420 K, but still far below the light-off temperature over the reference (500 K). The advantage of Pd/CZ in CO oxidation had completely disappeared (Fig. S9a), but with it also the low-temperature release of N_2O (Fig. S9d). Notably, the performance of Pd/CZ was affected also in other aspects. Its CO conversion curve was now suspended by a shoulder slightly above 60 % (much alike that of Au/CZ in Fig. 4a), which delayed full CO conversion stronger than over all other catalysts. In addition, while N_2O formation during light-off at 500-550 K tailed to higher temperatures over most initial catalysts (Fig. 4d), this effect was strongly enhanced just for Pd/CZ after stabilization (Fig. S9d). Based on the data of Fig. S9, the modification of Pd/CZ with small amounts of Au makes sense: despite minor deficits in the light-off temperature (not more than 10 K), $AuPd_4$/CZ kept its advantage of steep approach to 100 % conversion for propene and NO (Fig. S9b, c), though not for CO (Fig. S9a), and combined it with a steep decay of N_2O formation right above its maximum at ≈540 K (Fig. S9d).

On the LA support, the variation in the performance of the Au_xPd_y catalysts was much stronger than on CZ (Figure 5). The peculiar CO conversion curve of Au/LA (Fig. 5a) has been discussed in some detail in refs. [17] and [18]. The pronounced dip between 400 and 600 K is most likely due to the poisoning of the active support surface around Au by carbonaceous residues, which are burnt away above 500 K [18]. The expectation that Pd might help against the deposition of these species was not fulfilled. Instead, Au was very effectively poisoned by small amounts of Pd. Notably, the CO conversion curve of Au_3Pd/LA exhibited a minimum as well, decreasing after having achieved just 18 % before finally lighting off at 605 K. Such minimum can be also observed in the curve of AuPd/LA, but it faded out at high Pd content. On the whole, the result

with respect to CO oxidation in the TWC mixture is negative: Pd poisons Au, and Au poisons Pd. Reminiscent of some literature work on CO oxidation in a binary feed, the catalytic performance of the Au-rich bimetallic catalyst was the poorest in the series.

In propene oxidation (Fig. 5b) and NO reduction (Fig. 5c), the situation is less complex due to missing or less pronounced low-temperature conversion peaks. In propene oxidation, the relation between the metals is similar as in CO oxidation: Au poisons Pd, and Pd poisons even the rather low propene oxidation activity of gold. As a result, the range of light-off temperatures for propene oxidation is as wide as 115 K on LA, as compared to 43 K on the CZ support (Figs. 5b, 4b). The situation in NO conversion differs insofar as NO reduction activity of Au alone is too low to be effectively poisoned by Pd (Fig. 5c). Indeed, even very small Pd contents imparted the catalysts a NO reduction activity sufficient to achieve large conversions, though at high temperatures (T_{50} of Au_4Pd/LA – 658 K). The ranking of the remaining catalysts is as in propene oxidation.

In NO conversion, the Pd-rich catalysts exhibited a pronounced low-temperature peak, with high selectivity to N_2O (Fig. 5d). The spread between light-off temperatures for NO reduction (excluding the low-temperature peak of Pd/LA) is 142 K on LA, as compared to 52 K on CZ (Fig. 4c). Correspondingly, the high-temperature peaks of N_2O release related to NO light-off spread over 120 K.

For the LA-supported catalysts, similar stabilization tendencies were observed. A comparison of conversion curves measured with $AuPd_4$/LA in the initial state and after three runs – however, with a slightly lean mixture – reveals that low-temperature N_2O formation is suppressed by stabilization on this support as well (Figure S11).

3.2.2. After ageing at 1223 K

The performance of CZ- and LA-supported AuPd catalysts after ageing at 1223 K is summarized in Figures 6 and 7, respectively. The behavior of the reference catalyst after the

same ageing procedure is reported as well, and the conversion curves of the initial catalysts are repeated for comparison. The data for AuPd/CZ can be found in Figures S8 and S10.

As expected, the thermal stress caused serious losses in activity. Over the CZ-supported catalysts, the light-off temperatures of CO, propene, and NO conversion increased by 160 K, 60 K, and 70 K on average, respectively (Figure 6). However, all aged catalysts still outperformed the aged reference in CO oxidation, and all but Au/CZ and Au_4Pd/CZ in propene oxidation (Fig. 6a, b). In NO reduction, only the Pd-rich compositions were competitive, the remaining catalysts (including AuPd/CZ, Fig. S7c) dropped behind the reference TWC (Fig. 6c). Correspondingly, only the N_2O peaks of the Pd-rich samples appeared at lower temperatures than that of the reference (Fig. 6d). The N_2O release of the latter was dramatically suppressed by the thermal treatment, therefore, N_2O formation over the Pd-rich catalysts and over the reference TWC was on the same order of magnitude. Notably, a significantly enhanced N_2O release tailing to higher reaction temperatures was exhibited by AuPd/CZ (Fig. S8d) and by Au_4Pd/CZ (Fig. 6d).

In Fig. 6, all conversion curves of Pd/CZ, $AuPd_4$/CZ, and $AuPd_2$/CZ are close together while those of the remaining catalysts (including AuPd/CZ, Fig. S8c) are shifted to higher temperatures. Moreover, over wide temperature ranges, the curves of the Au-containing samples, which are almost indistinguishable, proceed at slightly lower temperatures than that of Pd/CZ. The light-off temperatures of these catalysts are decreased by 5-8 K. Apparently, the modification of Pd/CZ with small amounts of Au has a favorable effect on the catalyst stability.

Among the LA-supported samples, only the monometallic Pd/LA catalyst can compete with the reference after thermal ageing (Fig.7). The remaining catalysts stayed back behind the reference in the conversion of all reactants. The damage was most drastic in CO oxidation where the light-off temperatures of Pd/LA and $AuPd_4$/LA increased by ca. 200 K, and that of Au/LA by 150 K even if only the re-activation after the conversion dip is taken into account (Fig. 7a). For the remaining reactions, the losses were less dramatic, with average increases of T_{50} by 80 K both

for propene oxidation (except for Au/LA, Fig. 7b) and NO reduction (except for Au_3Pd/LA, Fig. 7c), slightly more than on the CZ support. In the Pd-rich LA-supported catalysts, thermal stress suppressed the disposition to N_2O formation even stronger than in the reference (Fig. 7d). As observed with the CZ-supported samples (Fig. 6d), N_2O formation increased with growing Au content. This can be clearly seen in the data of AuPd/LA (Fig. 7d), but the same N_2O selectivity (ca. 20 %) was also obtained at the peak NO conversion achieved by Au_3Pd/LA slightly above 800 K.

3.3. Gold as a poison and a promotor in Pd-Au three-way catalysts

The catalytic data presented in section 3.2 indicate that the proper use of gold in a three-way catalyst offers opportunities for improving the catalytic performance. The favorable effect of gold is, however, very different from expectations based on prior studies. It can be achieved only in a narrow range of catalyst compositions, which needs to be well specified to escape poisoning effects exerted by gold in a much wider range of catalyst compositions.

At a first glance, the AuPd system is dominated by poisoning rather than by promotion. The poisoning of Pd activity by gold is obvious. However, even Pd acts as a poison: it damages the oxidation activity of gold, most effectively on the LA support, on CZ only the activity for propene oxidation. On LA, the high CO oxidation activity of gold breaks down by adding just a few wt-% Pd (Fig. 5a), but the extent of poisoning shows that this palladium cannot even exhibit its own CO oxidation activity. At temperatures around 475 K, where Pd/LA achieves a CO conversion of 95 % with 2.2 wt-% Pd (cf. Table 1), a conversion of ca. 65 % would be expected on the basis of a first-order rate law from a catalyst containing one seventh of the Pd amount at comparable dispersion. The actual conversion was, however, 18 %, and it decreased with growing temperature in a range where Pd/CZ achieved full conversion (Fig. 5a). It has been proposed in literature that Au poisons the oxidation activity of Pd by destroying contiguous Pd sites required for O_2 activation [24, 65]. In the light of this idea, there must be a

close relation between Au and Pd in Au_3Pd/LA, although XRD detected only small amounts of Pd in bulk alloy structures (an average composition of $Au_{10}Pd$ was estimated from Fig. 1b). More Pd^0 might decorate the surfaces of Au particles, which are rather small in this catalyst, so that the abundance of contiguous ensembles of Pd^0 was low. With increasing Pd/Au ratio, bulk and surfaces of Au particles cannot bind all Pd atoms, which facilitates the formation of contiguous Pd metal sites allowing for a strongly enhanced oxidation activity. The Pd-Au interaction mentioned above might explain that an Au $4f_{7/2}$ binding-energy shift was also found for bimetallic CZ-supported catalysts, though of smaller size than in the LA-supported samples.

While the former discussion may be extended also to the tendencies in propene oxidation (Fig. 5b), the intermediate dip in CO conversion over all Au-containing bimetallic catalysts (Fig. 5a) deserves more attention. Its similarity with the minimum in CO conversion over Au/LA is spurious: it arises from Pd rather than from Au. Indeed, none of the bimetallic catalysts achieved any CO conversion below the onset temperature of Pd/LA: the CO oxidation activity of gold was completely killed by the palladium, probably by destroying the Au-support interaction. As mentioned above, some of the low-temperature CO conversion over Pd originates from the reduction of NO, mostly to N_2O (N_2O selectivity in the NO conversion peak is close to 90 %, cf. Figs. 5c, d). The decay of NO conversion above the peak temperature does probably not result from a lost competition for the reductant, but rather from thermal instability of a critical adsorbate. Over Pd-rich catalysts, the unreacted CO may be oxidized by O_2 instead in this temperature range, which mitigates the effect on CO conversion: its further increase is just delayed. Due to their lower oxidation activity, catalysts containing more gold are less capable to compensate the vanishing NO/CO reaction by CO oxidation, which results in more or less pronounced CO conversion dips. The upsurge of CO, propene, and NO conversions to 100 % started above 500 K, rather simultaneous for the Pd-rich samples. In the case of Au_3Pd/LA, the oxidation reactions clearly preceded the NO reduction. With the low-temperature CO oxidation

sites poisoned on both Au and Pd surfaces, this high-temperature increase of the oxidation rates seems to be due to an alternative reaction mechanism at least over this catalyst.

The major differences between LA- and CZ-supported catalysts certainly arise from the strong stabilization of Pd^{2+} by CeO_2-containing surfaces [62-64]. In the initial samples, Pd^{2+} and Pd^0 coexisted on both supports (Tables 4 and 3) despite the initial reduction in H_2 at 523 K. Irrespective of whether this is due to an incomplete reduction or to re-oxidation during storage, it proves a stabilization of Pd^{2+} by both supports: bulk PdO is reduced in hydrogen below 273 K [66], and the reverse is unlikely to happen at ambient without assistance by a stabilizer for Pd^{2+}. Although the relation between Pd^{2+} and Pd^0 in the initial catalysts suggests that the stabilization is stronger on CZ, the ultimate confirmation for this conclusion comes from the samples aged at 1223 K (Table 4, Fig. 2): while Pd was completely metallic (and alloyed) on LA, significant amounts of Pd remained cationic on CZ, and the Pd metal formed was not completely alloyed. The easy interchange between the +2 and 0 oxidation states on CZ competes also with the aggregation of Pd (cf. Pd dispersion on LA and CZ in Table 1) and with the tendency of Pd to interact with Au: while there is no indication of alloying (or even of interaction) in the diffractograms and the AuL_{III}-edge XANES of the CZ-supported catalysts (Figs. 1a, S7a), alloying is indicated by XRD already in the initial LA-supported samples (Fig. 1b), and changes can be clearly seen in the AuL_{III}-edge XANES (Fig. S7b), which are most likely caused by the influence of Pd.

The CO and propene conversion curves of the different CZ-supported catalysts are close together as might be expected when the differences are caused only by varying quantities of the active components (Fig. 4a, b). As mentioned above, the extra low-temperature CO conversion over Pd/CZ (and to some extent AuPd/CZ, Fig. S8a) arises from the capability of Pd to catalyze NO reduction to N_2O, which is also reflected by high NO conversions and N_2O releases in this temperature range. However, just the attenuation of low-temperature N_2O formation in most of the Au-containing catalysts (Fig. 4c, d) suggests that Au and Pd are not completely segregated

on the CZ support either. Indeed, the propene conversion curve of Au_4Pd/CZ lags behind that of Au/CZ (Fig. 4b), much as found with the Au-rich LA-supported catalysts (Fig. 5b). The rates of the high-temperature oxidation process are, however, much higher on CZ than on LA (T_{50} of Au_4Pd/CZ – 535 K, of Au_3Pd/LA – 625 K). As a result, the spread of the propene light-off temperatures over the whole series is smaller on CZ than on LA (Figs. 4b, 5b). On the other hand, the spread of the propene light-off temperatures on CZ is close to that of NO reduction, to which gold cannot contribute at all (Fig. 4b, c). By analogy, this suggests that Au does not contribute to the propene oxidation over Au_4Pd/CZ either. Together with the drastic differences between spread ranges on CZ and LA, this may suggest that both propene oxidation and NO reduction on the Au-rich catalysts proceed on isolated Pd atoms shuttling between Pd^0 and Pd^{2+} because this Pd oxidation is strongly favored on the surface of CZ.

Notably, the same Au-Pd interaction that resulted in delayed propene oxidation over the Au-rich catalysts (Figs. 4b, 5b) did not poison CO oxidation to any significant extent on CZ (Au_4Pd/CZ, Fig. 4a), while it killed the Au-related reaction completely in the case of Au_3Pd/LA (Fig. 5a). This difference suggests mechanistic differences also in CO oxidation over Au sites on the two supports. We will come back to this point in a subsequent paper on the basis of more evidence on structural properties.

The breakdown of the low-temperature N_2O formation over Pd/CZ after stabilization (Fig. S9) suggests that this feature may be caused by extremely disperse structures, which aggregate already under relatively mild conditions. In all reactions, activity decrease was stronger for higher Pd contents, which resulted in a further narrowing of the spread between light-off temperatures. In CO oxidation, it became less than 15 K. The outstanding performance just of Au/CZ and Au_4Pd/CZ in CO oxidation (Fig. S9a) emphasizes that there is no poisoning of Au sites for this reaction by Pd on CZ unlike on LA. The stronger impact of the stabilization on the Pd-rich preparations may result from the extremely high dispersion of Pd in the initial catalysts (Fig. 1a), which renders the Pd more prone to transient behavior than the bigger Au particles.

The catalytic properties of the aged LA-supported catalysts (Fig. 7) emphasize the unfavorable effects of alloying between Au and Pd, which are implied already by the data of the initial catalysts (Fig. 5). Opposed to this, the results of the CZ-supported catalysts reveal a surprising performance of the Pd-rich bimetallic samples that maintained a slightly higher residual activity than the monometallic Pd catalyst (Fig. 6). Even for a sceptic ascribing the lag of the latter to experimental scatter, the catalysts with Pd/Au ≥ 2 are indistinguishable, i.e., the performance of Pd/CZ can be achieved with 1 wt-% Pd instead of 2.2 wt-% (Table 1). In the specific relation between Pd and Au realized in these aged CZ-supported catalysts, Au is a promotor for Pd: its activity is inferior in CO and propene oxidation (Fig. 6a, b) and almost zero in NO reduction, but its influence increased the activity of Pd sites in Pd-rich preparations by more than 100 %.

Notably, this increase was absent in the initial catalysts (Fig. 4), where its presence might have suggested that it occurs without any assistance by gold, e.g. by smaller particle sizes at lower Pd contents. Now, the conversions of all three components clearly decrease with decreasing Pd content in the initial samples also on the CZ support. The improved behavior of the Pd-rich alloys is the result of the high-temperature treatment, which causes mobility of both Pd and Au as indicated by the increased sizes of metal particles (Figs. 1 and 2). It is, therefore, very likely that Au is indeed involved in the processes resulting in higher residual activity of the bimetallic catalysts, although it is as yet unclear, how this might occur. The characterization data reported in this paper just indicate a coexistence of Au-Pd alloy particles with Pd in segregated monometallic particles and in cationic form (Table 4, Fig. 2b). This is definitely insufficient to describe the obviously rather complex surface after ageing at 1223 K. We will come back to this problem on the basis of more comprehensive structural data in a subsequent paper, which will also be used to try and describe the state of CZ-supported Pd under reaction conditions and to discuss some mechanistic aspects only touched upon in this communication in some more detail.

4. Conclusions

The combination of Au with Pd does not remove the poisoning effects that restrain gold from exhibiting its high oxidation activity in reaction environments typical for three-way catalysis. Instead, Au poisons both the oxidation and the NO reduction activity of Pd. This poisoning is most pronounced on a La_2O_3/Al_2O_3 support (LA), but only minor on a Ce-Zr mixed-oxide support (CZ).

Therefore, all CZ-supported Pd and Au-Pd catalysts studied were superior to a commercial reference in oxidation and most of them also in the NO reduction. After an ageing treatment (5 % O_2, 10 % H_2O in He, 6 h at 1223 K), the poisoning influence of Au was just aggravated on the LA support, while the residual activity of Pd-rich Au-Pd/CZ catalysts was the same as (or better than) that of Pd/CZ, although Au does not contribute significantly to NO reduction and propene oxidation under the given reaction conditions. Allowing for identical activity with less than 50 % of the Pd in Pd/CZ, Au turned out to operate as a promotor in these catalysts, with all of them outperforming the aged reference sample.

Characterization shows a stabilization of Pd in the +2 oxidation state on CZ, most likely by a specific interaction between CeO_x and Pd^{2+}. The resulting facile oxidation of Pd^0 and the delay of alloy formation between Pd and Au are major reasons for the different support influences by LA and CZ. While Pd was found only partially reduced on both supports initially, significant alloy formation could be detected on LA, but not on CZ, where details of the catalytic results nevertheless suggested the existence of Pd-Au interactions, maybe via decoration. After ageing at 1223 K (above the decomposition temperature of PdO), Pd was completely metallic and alloyed on LA, while Pd^{2+} still coexisted with (alloyed) Pd^0 on CZ. More characterization work will be, however, necessary to elucidate the relation between the surface structure and the transformation of Au from a poison into a promotor.

Acknowledgements

We gratefully acknowledge financial support by the German Science Foundation (DFG, Grant No. Gr 1447/24-2), by the Ministry of Science and Higher Education of the Russian Federation (project AAAA-A-17-117041710079-8), and by the European Research Council (ERC-725915, OPERANDOCAT). We are grateful to Ms. N. Arshadi and Dr. I. Kraevskaya for their experimental support, beamline scientists Dr. Edmund Welter (Desy Hamburg) and Dr. Roman Chernikov (CLS) for their help at the synchrotrons, and Prof. A. Lisitsyn and Dr. D. Zyuzin for valuable discussion. We also thank Sasol Germany GmbH and Umicore & Co. KG Hanau (Germany) for donations of supports.

Table 1 – Metal loadings, particle sizes (TEM) and Pd dispersion (CO chemisorption) of supported AuPd catalysts

Sample code	Wt.% Au	Wt.% Pd	Atom-%[a] Au	Atom-%[a] Pd	Average particle diameter[b], $d_l \pm \sigma$, nm	Pd dispersion[c] f_{Pd} [$f_{Pd,corr}$][d]
Au/LA	1.8	-	1		1.7 ± 0.3	
Au_3Pd/LA	1.8	0.3	0.76	0.24	1.6 ± 0.3	0.29 [n. a.]
AuPd/LA	1.2	0.6	0.51	0.49	2.6 ± 1.0	0.34 [0.5]
$AuPd_4$/LA	0.6	1.2	0.21	0.79	3.2 ± 1.2	0.26 [0.4]
Pd/LA	-	2.1		1	2.4 ± 0.6	0.32 [0.6]
Au/CZ	1.6	-	1		2.8 ± 0.6	
Au_4Pd/CZ	2.1	0.3	0.79	0.21	3.3 ± 0.7	0.38 [1.3]
AuPd/CZ	1.6	0.6	0.59	0.41	2.9 ± 0.8	0.51 [1.1]
$AuPd_2$/CZ	1.0	1.0	0.35	0.65	1.1 ± 0.2	0.52 [1.0]
$AuPd_4$/CZ	0.7	1.5	0.20	0.80	2.7 ± 0.7	0.51 [n. a]
Pd/CZ	-	2.2		1	1.2 ± 0.3	0.46 [1.2]

[a]related to noble metal content [b]$d_l = \sum d_i/N$, N – number of particles included, σ – standard deviation; for averaged according to different weightings see supporting information, [c] $f_{Pd} = n(exposed)/n(total)$, n … number of atoms

[d] $f_{Pd,corr} = f_{Pd}\, n_{Pd}/n_{Pd^{2+}}$, with $n_{Pd^{2+}}$ derived from XANES

Table 2 – Texture data of catalysts after preparation and after ageing at 1223 K

Catalysts	Surface area[a], m^2/g	Mean pore diameter[a], nm	Total pore volume[a], cm^3/g
Au/LA	135	13.3	0.45
AuPd/LA	130 [86]	10.0 [18.2]	0.40 [0.39]
$AuPd_4$/LA	127 [84]	10.0 [17.9]	0.41 [0.38]
Au/CZ	65	14.8	0.24
Au_4Pd/CZ	61 [24]	15.1 [18.8]	0.20 [0.11]
AuPd/CZ	61 [22]	15.1 [17.8]	0.21 [0.10]
$AuPd_4$/CZ	54 [22]	15.1 [17.8]	0.20 [0.10]

[a]value after preparation [after ageing at 1223 K]

Table 3 – XPS binding energies and atomic ratios of the supported AuPd catalysts, surface concentrations compared with bulk concentrations

…/LA	BE, eV			Atomic ratios[c]					…/CZ	BE, eV	Atomic ratio[d]	
	Au^{a}	$Pd^{0,b}$	$Pd^{2+,b}$	Pd^{2+}/Pd^{0}	$(Au/Al)_S$	$(Au/Al)_B$	$(Pd/Al)_S$	$(Pd/Al)_B$		Au^{a}	$(Au/CZ)_S$	$(Au/CZ)_B$
Au	83.8	-	-	-	0.0037	0.0048	-	-	Au	83.9	0.040	0,.012
Au_3Pd	83.4	334.6	336.0	0.53	0.0033	0.0048	0.0018	0.016	Au_4Pd	83.7	0.047	0.016
AuPd	83.5	334.5	336.0	0.54	0.0030	0.0032	0.0029	0.027	AuPd	83.7_5	0.048	0.013
									$AuPd_2$	83.7	0.040	0.0082
$AuPd_4$	83.4	334.4	336.0	0.85	0.0012	0.0016	0.0057	0.058	$AuPd_4$	83.6_5	0.053	0,0051
Pd	-	334.9	336.6	0.65	-		0.011	0.011	Pd	-	-	-

[a]Au $4f_{7/2}$ [b]Pd $3d_{5/2}$ [c]S – surface (XPS), B – bulk (XRF) [c]Au/(Ce + Zr)

Table 4 – Chemical state (content in %) of Pd as derived from linear combination analysis of the XANES spectra in Figure 3

Catalyst	Initial state		Aged at 1223 K	
	Pd^{2+}	Pd^{0}	Pd^{2+}	Pd^{0}
Pd/LA	45	55	0	100
$AuPd_4$/LA	35	65	0	100
AuPd/LA	35	65	0	100
Pd/CZ	60	40	50	50
$AuPd_4$/CZ	n. a.	n. a	20	80
$AuPd_2$/CZ	50	50	60	40
AuPd/CZ	55	45	40	60
Au_4Pd/CZ	70	30	n. a.	n. a.

References

[1] M.V. Twigg, Progress and future challenges in controlling automotive exhaust gas emissions, Appl. Catal. B 70 (2007) 2-15.

[2] F. Haass, H. Fuess, Structural characterization of automotive catalysts, Adv. Eng. Mat. 7 (2005) 899-913.

[3] R.M. Heck, R.J. Farrauto, S.T. Gulati, Catalytic Air Pollution Control: Commercial Technology, 3rd ed., John Wiley & Sons, New York, 2009.

[4] G.C. Bond, C. Louis, D.T. Thompson, Catalyis by Gold, Imperial College Press, London, 2006.

[5] C. Cellier, S. Lambert, E.M. Gaigneaux, C. Poleunis, V. Ruaux, P. Eloy, C. Lahousse, P. Bertrand, J.P. Pirard, P. Grange, Investigation of the preparation and activity of gold catalysts in the total oxidation of n-hexane, Appl. Catal. B 70 (2007) 406-416.

[6] E. Seker, E. Gulari, Single step sol-gel made gold on alumina catalyst for selective reduction of NOx under oxidizing conditions: Effect of gold precursor and reaction conditions, Appl. Catal. A 232 (2002) 203-217.

[7] F. Cosandey, T.E. Madey, Growth, morphology, interfacial effects and catalytic properties of Au on TiO_2, Surf. Rev. Lett. 8 (2001) 73-93.

[8] S. Ivanova, C. Petit, V. Pitchon, Application of heterogeneous gold catalysis with increased durability: Oxidation of CO and hydrocarbons at low temperature, Gold Bull. 39 (2006) 3-8.

[9] G.M. Veith, A.R. Lupini, S. Rashkeev, S.J. Pennycook, D.R. Mullins, V. Schwartz, C.A. Bridges, N.J. Dudney, Thermal stability and catalytic activity of gold nanoparticles supported on silica. J. Catal. 262 (2009) 92-101.

[10] I.L. Simakova, Y.S. Solkina, B.L. Moroz, O.A. Simakova, S.I. Reshetnikov, I.P. Prosvirin, V.I. Bukhtiyarov, V.N. Parmon, D.Y. Murzin, Selective vapour-phase alpha-pinene isomerization to camphene over gold-on-alumina catalyst, Appl. Catal. A 385 (2010) 136-143.

[11] T. Akita, M. Kohyama, M. Haruta, Electron Microscopy Study of Gold Nanoparticles Deposited on Transition Metal Oxides, Acc. Chem. Res. 46 (2013) 1773-1782.

[12] N. Masoud, T. Partsch, K.P. de Jong, P.E. de Jongh, Thermal stability of oxide-supported gold nanoparticles, Gold Bull. 52 (2019) 105-114.

[13] J.R. Mellor, A.N. Palazov, B.S. Grigorova, J.F. Greyling, K. Reddy, M.P. Letsoalo, J.H. Marsh, The application of supported gold catalysts to automotive pollution abatement, Catal. Today 72 (2002) 145-156.

[14] G. Pattrick, E. van der Lingen, C.W. Corti, R.J. Holliday, D.T. Thompson, The potential for use of gold in automotive pollution control technologies: a short review, Top. Catal. 30-31 (2004) 273-279.

[15] M.S. Scurrell, Thoughts on the use of gold-based catalysts in environmental protection catalysis, Gold Bull. 50 (2017) 77-84.

[16] Y. Zhang, R.W. Cattrall, I.D. McKelvie, S.D. Kolev, Gold, an alternative to platinum group metals in automobile catalytic converters, Gold Bull. 44 (2011) 145.

[17] V. Ulrich, B. Moroz, I. Sinev, P. Pyriaev, V.I. Bukhtiyarov, W. Grünert, Studies on Three-way Catalysis with Supported Gold Catalysts. Influence of Support and Water Content in Feed, Appl. Catal. B 203 (2017) 572-581.

[18] V. Ulrich, C. Froese, B. Moroz, P. Pyrjaev, E. Gerasimov, I. Sinev, B. Roldan Cuenya, M. Muhler, V. Bukhtiyarov, W. Grünert, Three-way catalysis with supported gold catalysts: Poisoning effects of hydrocarbons, Appl. Catal. B 237 (2018) 1021-1032.

[19] B.L. Moroz, K.C.C. Kharash, M.Y. Smirnov, A.S. Bobrin, V. I. Bukhtiyarov, US Patent No. 7,824,639 B2, 2010.

[20] E.G. Allison, G.C. Bond, The Structure and Catalytic Properties of Palladium-Silver and Palladium-Gold Alloys, Catal. Rev. 7 (1972) 233-289.

[21] F. Gao, Y. Wang, D.W. Goodman, CO Oxidation over AuPd(100) from Ultrahigh Vacuum to Near-Atmospheric Pressures: CO Adsorption-Induced Surface Segregation and Reaction Kinetics, J. Phys. Chem. C 113 (2009) 14993-15000.

[22] A.M. Venezia, L.F. Liotta, G. Pantaleo, V. La Parola, G. Deganello, A. Beck, Z. Koppany, K. Frey, D. Horvath, L. Guczi, Activity of SiO_2- supported gold-palladium catalysts in CO oxidation, Appl. Catal. A 251 (2003) 359-368.

[23] K. Qian, W. Huang, Au-Pd alloying-promoted thermal decomposition of PdO supported on SiO_2 and its effect on the catalytic performance in CO oxidation, Catal. Today 164 (2011) 320-324.

[24] K. Qian, L. Luo, Z. Jiang, W. Huang, Alloying Au surface with Pd reduces the intrinsic activity in catalyzing CO oxidation, Catal. Today 280 (2017) 253-258.

[25] J. Xu, T. White, P. Li, C. He, J. Yu, W. Yuan, Y.-F. Han, Biphasic Pd-Au Alloy Catalyst for Low-Temperature CO Oxidation, J. Am. Chem. Soc. 132 (2010) 10398-10406.

[26] T. Ward, L. Delannoy, R. Hahn, S. Kendell, C.J. Pursell, C. Louis, B.D. Chandler, Effects of Pd on Catalysis by Au: CO Adsorption, CO Oxidation, and Cyclohexene Hydrogenation by Supported Au and Pd-Au Catalysts, ACS Catalysis 3 (2013) 2644-2653.

[27] Z. Suo, C. Ma, M. Jin, T. He, L. An, The active phase of Au-Pd/Al_2O_3 for CO oxidation, Catal. Comm. 9 (2008) 2187-2190.

[28] L. Guczi, A. Beck, A. Horvath, Z. Koppany, G. Stefler, K. Frey, I. Sajo, O. Geszti, D. Bazin, J. Lynch, AuPd bimetallic nanoparticles on TiO_2: XRD, TEM, in situ EXAFS studies and catalytic activity in CO oxidation, J. Mol. Catal. A 204 (2003) 545-552.

[29] A. Beck, A. Horváth, Z. Schay, G. Stefler, Z. Koppány, I. Sajó, O. Geszti, L. Guczi, Sol derived gold-palladium bimetallic nanoparticles on TiO_2: structure and catalytic activity in CO oxidation, Top. Catal. 44 (2007) 115-121.

[30] J.H. Carter, S. Althahban, E. Nowicka, S.J. Freakley, D.J. Morgan, P.M. Shah, S. Golunski, C.J. Kiely, G.J. Hutchings, Synergy and Anti-Synergy between Palladium and Gold in Nanoparticles Dispersed on a Reducible Support, ACS Catalysis 6 (2016) 6623-6633.

[31] C.M. Olmos, L.E. Chinchilla, J.J. Delgado, A.B. Hungría, G. Blanco, J.J. Calvino, X. Chen, CO Oxidation over Bimetallic Au-Pd Supported on Ceria-Zirconia Catalysts: Effects of Oxidation Temperature and Au:Pd Molar Ratio, Catal. Lett. 146 (2016) 144-156.

[32] T. Barakat, J.C. Rooke, H.L. Tidahy, M. Hosseini, R. Cousin, J.-F. Lamonier, J.-M. Giraudon, G. De Weireld, B.-L. Su, S. Siffert, Noble-Metal-Based Catalysts Supported on Zeolites and Macro-Mesoporous Metal Oxide Supports for the Total Oxidation of Volatile Organic Compounds, ChemSusChem 4 (2011) 1420-1430.

[33] M. Hosseini, T. Barakat, R. Cousin, A. Aboukais, B.L. Su, G. De Weireld, S. Siffert, Catalytic performance of core-shell and alloy Pd-Au nanoparticles for total oxidation of VOC: The effect of metal deposition. Appl. Catal.B 111-112 (2012) 218-224.

[34] A.N. Simonov, P.A. Pyrjaev, B.L. Moroz, V.I. Bukhtiyarov, V.N. Parmon, Electrodeposited Pd Sub-Monolayers on Carbon-Supported Au Particles of Few Nanometers in Size: Electrocatalytic Activity for Hydrogen Oxidation and CO Tolerance vs. Pd Coverage, Electrocatalysis 3 (2012) 119-131.

[35] J.K. Edwards, B. Solsona, P. Landon, A.F. Carley, A. Herzing, M. Watanabe, C.J. Kiely, G.J. Hutchings, Direct synthesis of hydrogen peroxide from H_2 and O_2 using Au-Pd/Fe_2O_3 catalysts, J. Mat. Chem. 15 (2005) 4595-4600.

[36] X. Wei, X.-F. Yang, A.-Q. Wang, L. Li, X.-Y. Liu, T. Zhang, C.-Y. Mou, J. Li, Bimetallic Au-Pd Alloy Catalysts for N_2O Decomposition: Effects of Surface Structures on Catalytic Activity, J. Phys. Chem. C 116 (2012) 6222-6232.

[37] H.U. Shin, D. Lolla, Z. Nikolov, G.G. Chase, Pd-Au nanoparticles supported by TiO_2 fibers for catalytic NO decomposition by CO, J. Ind. Eng. Chem. 33 (2016) 91-98.

[38] D.I. Enache, J.K. Edwards, P. Landon, B. Solsona-Espriu, A.F. Carley, A.A. Herzing, M. Watanabe, C.J. Kiely, D.W. Knight, G.J. Hutchings, Solvent-free oxidation of primary alcohols to aldehydes using Au-Pd/TiO_2 catalysts. Science 311 (2006) 362-365.

[39] L. Kesavan, R. Tiruvalam, M.H. Ab Rahim, M.I. bin Saiman, D.I. Enache, R.L. Jenkins, N. Dimitratos, J.A. Lopez-Sanchez, S.H. Taylor, D.W. Knight, C.J. Kiely, G.J. Hutchings, Solvent-Free Oxidation of Primary Carbon-Hydrogen Bonds in Toluene Using Au-Pd Alloy Nanoparticles, Science 331 (2011) 195-199.

[40] X. Wang, N.S. Venkataramanan, H. Kawanami, Y. Ikushima, Selective oxidation of styrene to acetophenone over supported Au-Pd catalyst with hydrogen peroxide in supercritical carbon dioxide, Green Chemistry 9 (2007) 1352-1355.

[41] Hao, X.H., Sharma, R., McCool, G., Harrison, B., Wahl, D., US-Patent 2013/0331258A1, 12. 12. 2013

[42] D. Cheng, H. Xu, A. Fortunelli, Tuning the catalytic activity of Au-Pd nanoalloys in CO oxidation via composition, J. Catal. 314 (2014) 47-55.

[43] J. Zhang, H. Jin, M.B. Sullivan, F.C.H. Lim, P. Wu, Study of Pd-Au bimetallic catalysts for CO oxidation reaction by DFT calculations, Phys. Chem. Chem. Phys.11 (2009) 1441-1446.

[44] F. Gao, Y. Wang, D.W. Goodman, CO/NO and CO/NO/O_2 reactions over a Au-Pd single crystal catalyst, J. Catal. 268 (2009) 115-121.

[45] J. Barbier, P. Marécot, G. Del Angel, P. Bosch, J.P. Boitiaux, B. Didillon, J.M. Dominguez, I. Schiftef, G. Espmosa, Preparation of platinum-gold bimetallic catalysts by redox reactions, Appl. Catal. A 116 (1994) 179-186.

[46] M. Bonarowska, J. Pielaszek, W. Juszczyk, Z. Karpinski, Characterization of Pd-Au/SiO_2 Catalysts by X-ray Diffraction, Temperature-Programmed Hydride Decomposition, and Catalytic Probes, J. Catal. 195 (2000) 304-315.

[47] S. Tsubota, M. Haruta, T. Kobayashi, A. Ueda, Y. Nakahara, Preparation of highly dispersed gold on titanium and magnesium-oxide,Stud. Surf. Sci. Catal. 63 (1991) 695-704.

[48] B.L. Moroz, P.A. Pyrjaev, V.I. Zaikovskii, V.I. Bukhtiyarov, Nanodispersed Au/Al_2O_3 catalysts for low-temperature CO oxidation: Results of research activity at the Boreskov Institute of Catalysis, Catal. Today 144 (2009) 292-305.

[49] K.M. Kaprielova, O.A. Yakovina, I.I. Ovchinnikov, S.V. Koscheev, A.S. Lisitsyn, Preparation of platinum-on-carbon catalysts via hydrolytic deposition: Factors influencing the deposition and catalytic properties, Appl. Catal. A 449 (2012) 203-214.

[50] J.H. Scofield, Hartree-Slater Subshell Photoionization Cross-Sections at 1254 and 1487 eV, J. Electron Spectrosc. Relat. Phenom. 8 (1976) 129-137.

[51] B. Ravel, M. Newville, ATHENA, ARTEMIS, HEPHAESTUS: data analysis for X-ray absorption spectroscopy using IFEFFIT, J. Synchrotron Radiat. 12 (2005), 537-541.

[52] P.A. Pyryaev, B.L. Moroz, D.A. Zyuzin, A.V. Nartova, V.I. Bukhtiyarov, Au/C catalyst obtained from a tetraamminegold(III) precursor: Synthesis, characterization, and catalytic activity in low-temperature CO oxidation, Kinet. Catal.51 (2010) 885-892.

[53] P. Riello, P. Canton, A. Benedetti, Au/C Catalyst: Experimental Evidence of the Coexistence of Nanoclusters and Larger Au Particles, Langmuir, 14 (1998) 6617-6619.

[54] P. Riello, P. Canton, A. Minesso, F. Pinna, A. Benedetti, Low-loaded metal Pd-Au supported catalysts on active carbon. Recent developments of the X-ray diffraction analysis to detect simultaneously nanoclusters and larger particles, in: A. Corma, F.V. Melo, S. Mendioroz, J.L.G. Fierro (Eds.) Studies in Surface Science and Catalysis, Elsevier2000, pp. 3273-3278.

[53] P.A.P. Nascente, S.G.C. Decastro, R. Landers, G.G. Kleiman, X-ray photoemission and Auger energy shifts in some gold-palladium alloys, Phys.Rev. B 43 (1991) 4659-4666.

[54] Y.S. Lee, Y.D. Chung, K.Y. Lim, C.N. Whang, Y. Jeon, B.S. Choi, A study of the electronic structure of Co-Pt alloys. J. Korean Phys. Soc. 35 (1999) S560-S563.

[55] C.W. Yi, K. Luo, T. Wei, D.W. Goodman, The composition and structure of Pd-Au surfaces, J. Phys. Chem. B 109 (2005) 18535-18540.

[56] J. Xu, T. White, P. Li, C.H. He, J.G. Yu, W.K. Yuan, Y.F. Han, Biphasic Pd-Au Alloy Catalyst for Low-Temperature CO Oxidation, J. Am. Chem. Soc. 132 (2010) 10398-10406.

[57] A.V. Bukhtiyarov, I.P. Prosvirin, V.I. Bukhtiyarov, XPS/STM study of model bimetallic Pd-Au/HOPG catalysts, Appl. Surf. Sci. 367 (2016) 214-221.

[58] A.V. Bukhtiyarov, I.P. Prosvirin, A.A. Saraev, A.Y. Klyushin, A. Knop-Gericke, V.I. Bukhtiyarov, In situ formation of the active sites in Pd-Au bimetallic nanocatalysts for

CO oxidation: NAP (near ambient pressure) XPS and MS study, Faraday Discuss. 208 (2018) 255-268.

[59] Y. Nagai, T. Hirabayashi, K. Dohmae, N. Takagi, T. Minami, H. Shinjoh, S. Matsumoto, Sintering inhibition mechanism of platinum supported on ceria-based oxide and Pt-oxide - support interaction, J. Catal. 242 (2006) 103-109.

[60] S. Colussi, A. Gayen, M. Farnesi Camellone, M. Boaro, J. Llorca, S. Fabris, A. Trovarelli, Nanofaceted Pd-O Sites in Pd-Ce Surface Superstructures: Enhanced Activity in Catalytic Combustion of Methane, Angew. Chem. Intern. Ed. 48 (2009) 8481-8484.

[61] S. Hinokuma, H. Fujii, M. Okamoto, K. Ikeue, M. Machida, Metallic Pd Nanoparticles Formed by Pd-O-Ce Interaction: A Reason for Sintering-Induced Activation for CO Oxidation, Chem. Mat. 22 (2010) 6183-6190.

[62] A. Satsuma, K. Osaki, M. Yanagihara, J. Ohyama, K. Shimizu, Low temperature combustion over supported Pd catalysts - Strategy for catalyst design, Catal. Today 258 (2015) 83-89.

[63] Z. Li, F. Gao, W.T. Tysoe, Carbon Monoxide Oxidation over Au/Pd(100) Model Alloy Catalysts, J. Phys. Chem. C 114 (2010) 16909-16916.

[64] S. Lin, L. Yang, X. Yang, R. Zhou, Redox properties and metal-support interaction of $Pd/Ce_{0.67}Zr_{0.33}O_2$-Al_2O_3 catalyst for CO, HC and NO_x elimination, Appl. Surf. Sci. 305 (2014) 642-649.

Figure captions

Figure 1 - X-ray diffractograms of supported Pd, Au, and AuPd catalysts in the initial state (after reduction at 523 K and storage); support diffractogram added for comparison; a – CeZrOx support (CZ), b – La-Al_2O_3 support (LA).

Figure 2 – X-ray diffractograms of supported Pd, Au, and AuPd catalysts after ageing in 5 % O_2, 10 % H_2O, balance He at 1223 K for 6 h; a – $CeZrO_x$ support (CZ), b – La-Al_2O_3 support (LA); signal at $2\theta \approx 85$ ° in b originates from support (cf. Figure 1).

Figure 3 – PdK-XANES spectra of supported Pd and AuPd catalysts in the initial state (a - CZ-supported catalysts, b - LA-supported catalysts) and after oxidative ageing at 1223 K (c - CZ-supported catalysts, d - LA-supported catalysts).

Figure 4 – Catalytic performance of CZ- supported Pd, Au, and AuPd catalysts in the conversion of a TWC model feed, compared with the performance of a commercial reference ("Ref"); conversions of CO (a), of propene (b), of NO (c), N_2O formation (d)

Figure 5 – Catalytic performance of LA-supported Pd, Au, and AuPd catalysts in the conversion of a TWC model feed, compared with the performance of a commercial reference ("Ref"); conversions of CO (a), of propene (b), of NO (c), N_2O formation (d).

Figure 6 – Influence of ageing at 1223 K on the catalytic performance of CZ-supported Pd, Au, and AuPd catalysts and of a commercial reference in the conversion of a TWC model feed; conversions of CO (a), of propene (b), of NO (c), N2O formation (d).

Figure 7 – Influence of ageing at 1223 K on the catalytic performance of LA-supported Pd, Au, and AuPd catalysts and of a commercial reference in the conversion of a TWC model feed; conversions of CO (a), of propene (b), of NO (c), N2O formation (d).

Figure 1 – X-ray diffractograms of supported Pd, Au, and AuPd catalysts in the initial state (after reduction at 523 K and storage); support diffractogram added for comparison; a – $CeZrO_x$ support (CZ), b – La-Al_2O_3 support (LA)

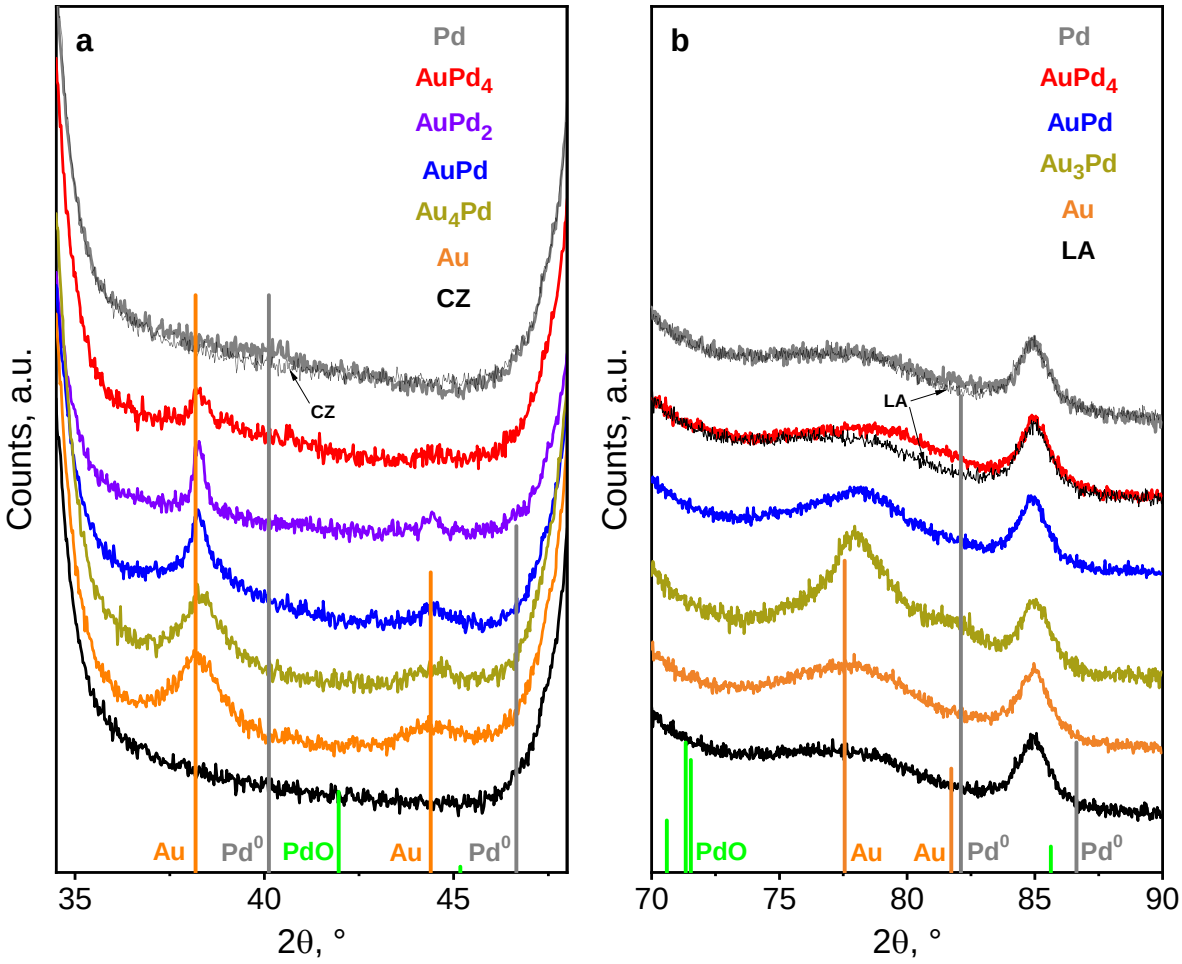

Figure 2 – X-ray diffractograms of supported Pd, Au, and AuPd catalysts after ageing in 5 % O_2, 10 % H_2O, balance He at 1223 K for 6 h; a – $CeZrO_x$ support (CZ), b – La-Al_2O_3 support (LA); signal at 2θ ≈ 85 ° in b originates from support (cf. Figure 1).

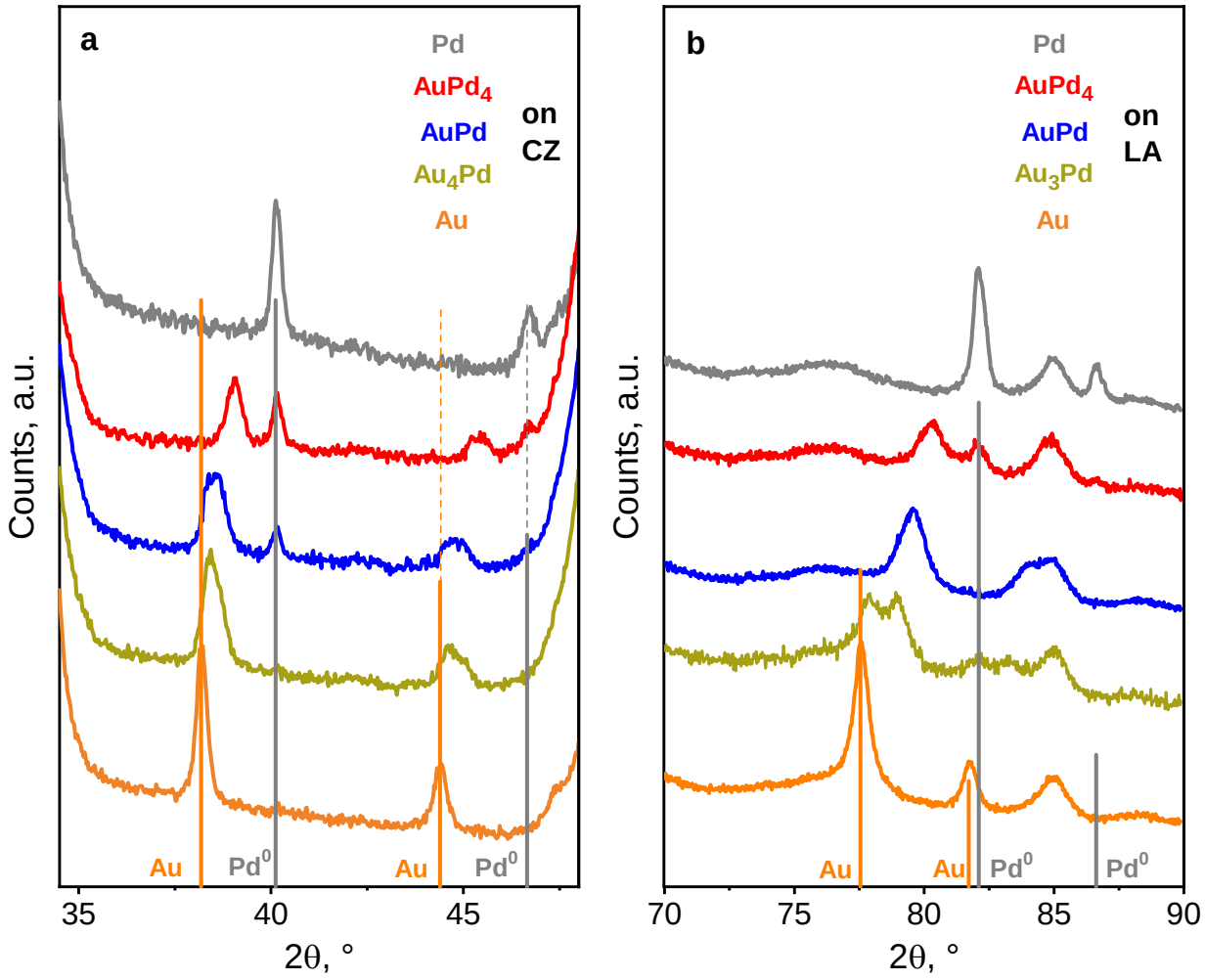

Figure 3 – Pd*K*-XANES spectra of supported Pd and AuPd catalysts in the initial state (a - CZ-supported catalysts, b - LA-supported catalysts) and after oxidative ageing at 1223 K (c - CZ-supported catalysts, d - LA-supported catalysts)

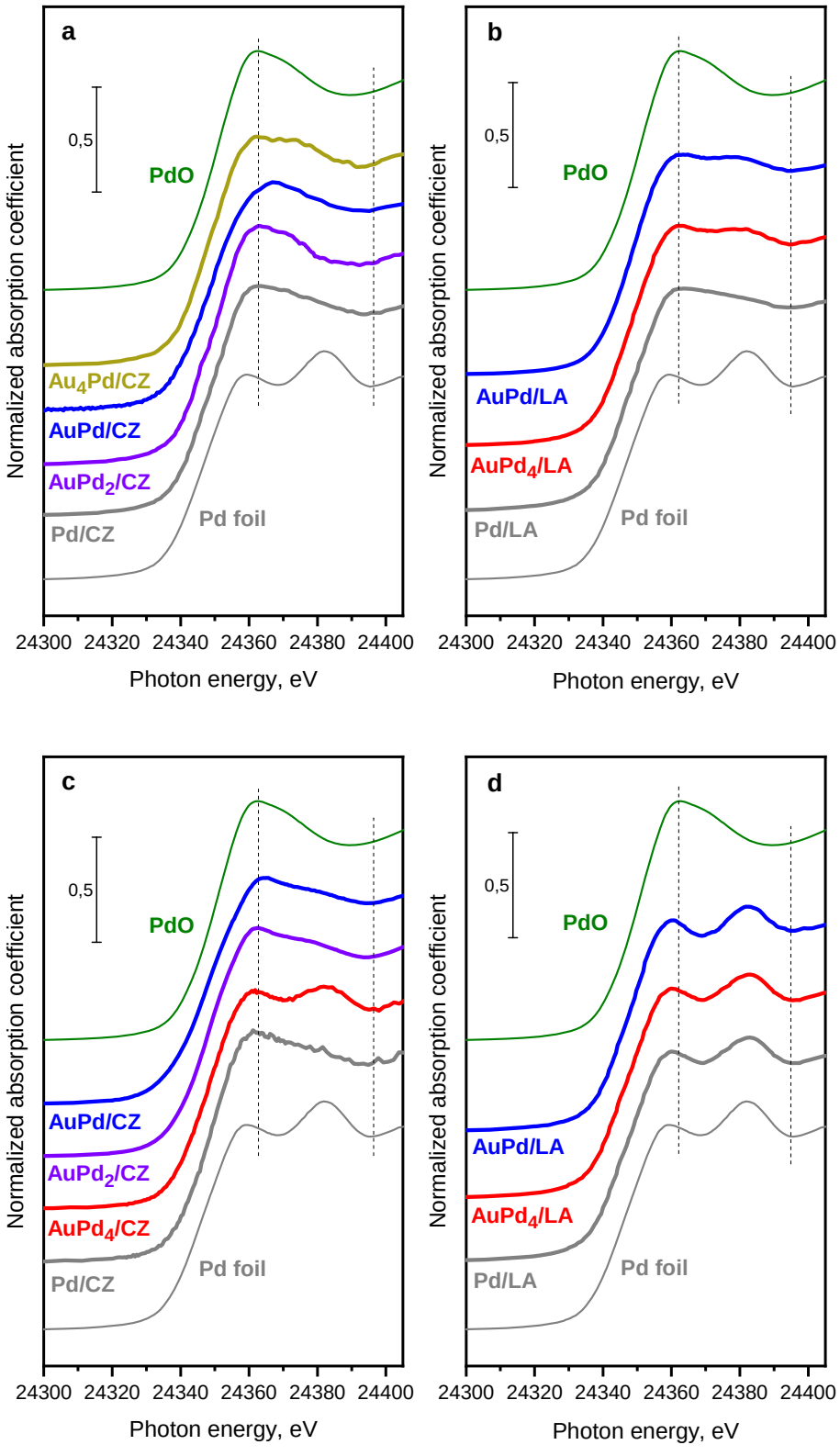

Figure 4 – Catalytic performance of CZ- supported Pd, Au, and AuPd catalysts in the conversion of a TWC model feed, compared with the performance of a commercial reference ("Ref"); conversions of CO (a), of propene (b), of NO (c), N_2O formation (d)

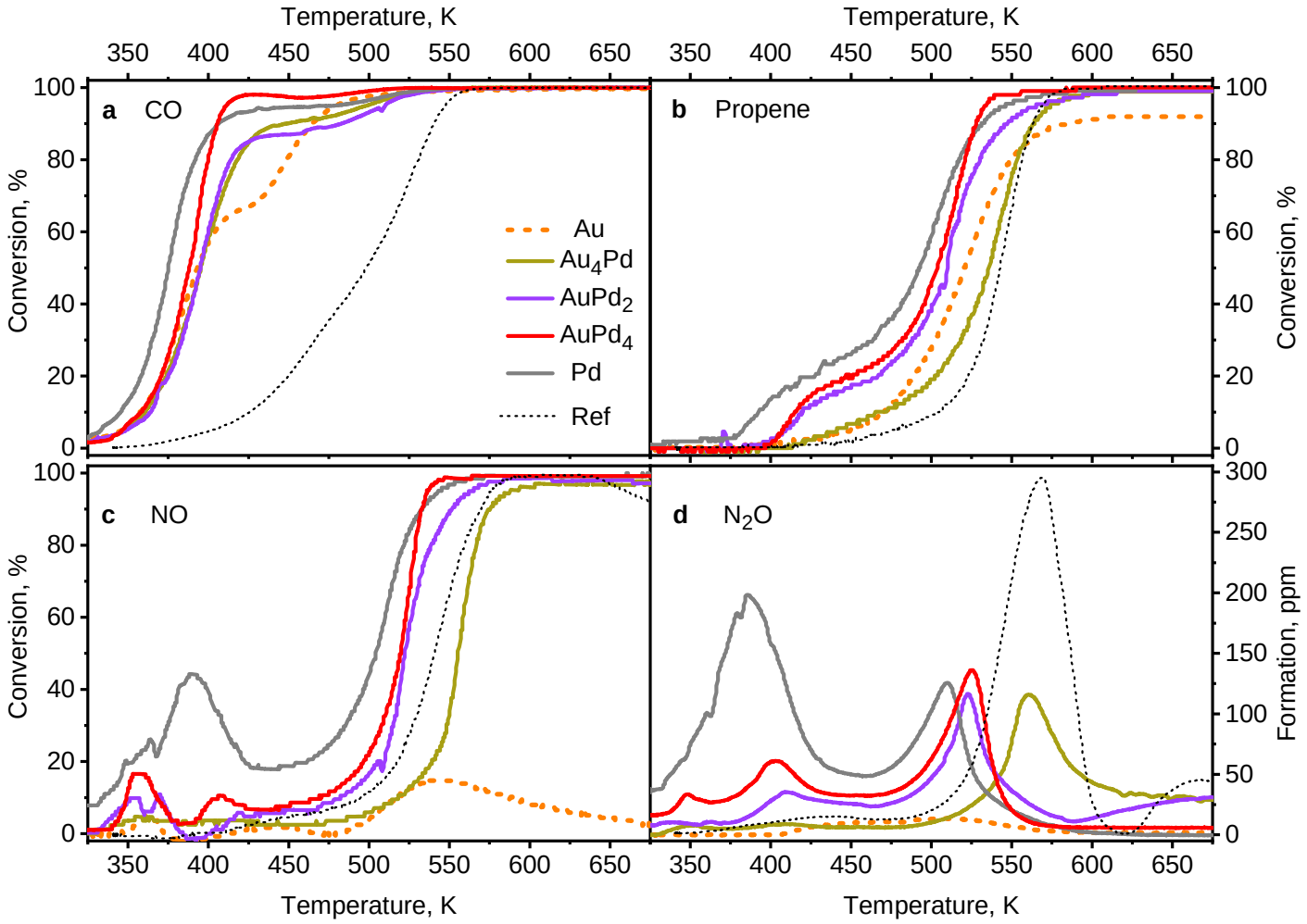

Figure 5 – Catalytic performance of LA- supported Pd, Au, and AuPd catalysts in the conversion of a TWC model feed, compared with the performance of a commercial reference ("Ref"); conversions of CO (a), of propene (b), of NO (c), N_2O formation (d).

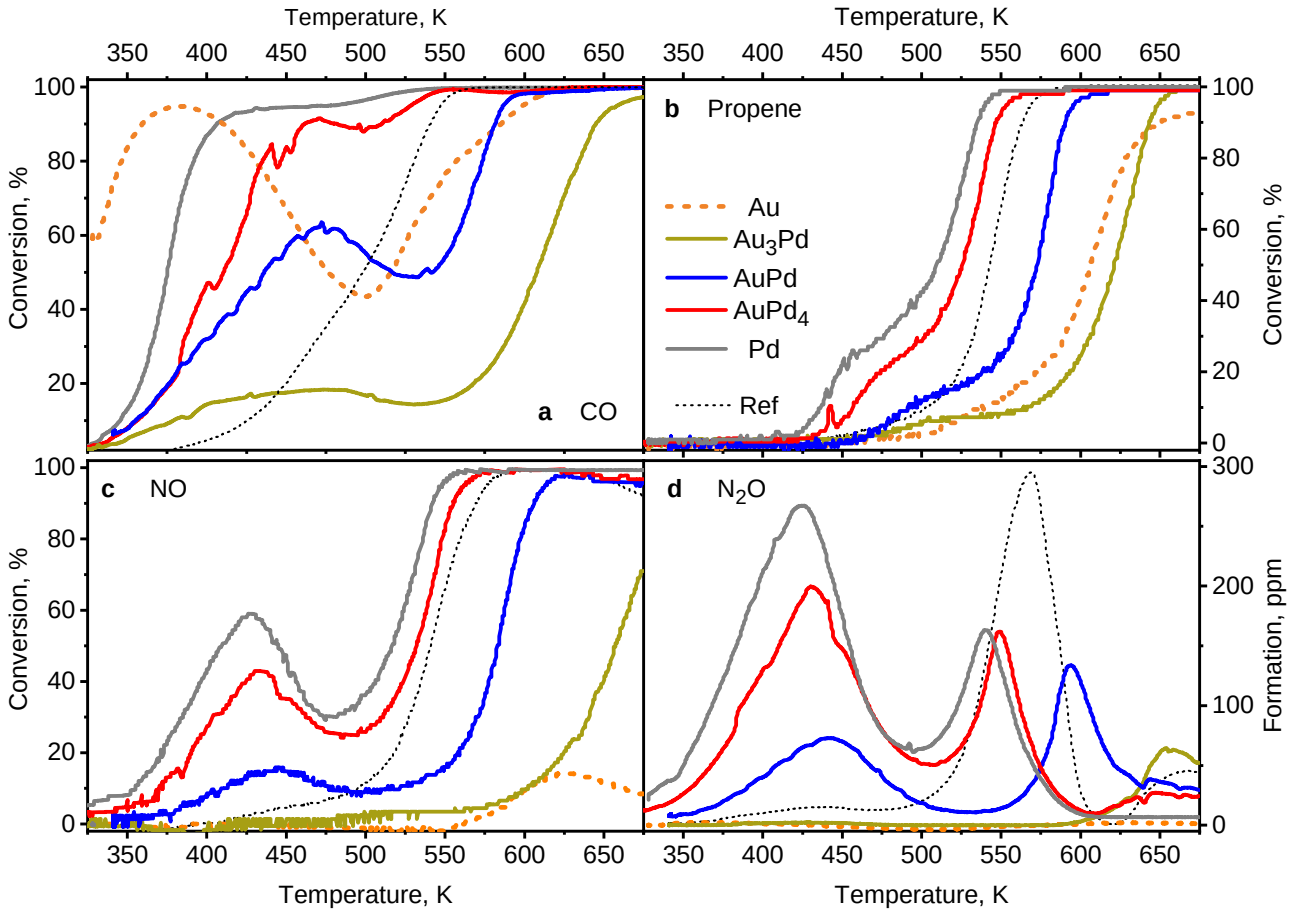

Figure 6 – Influence of ageing at 1223 K on the catalytic performance of CZ-supported Pd, Au, and AuPd catalysts and of a commercial reference in the conversion of a TWC model feed; conversions of CO (a), of propene (b), of NO (c), N_2O formation (d).

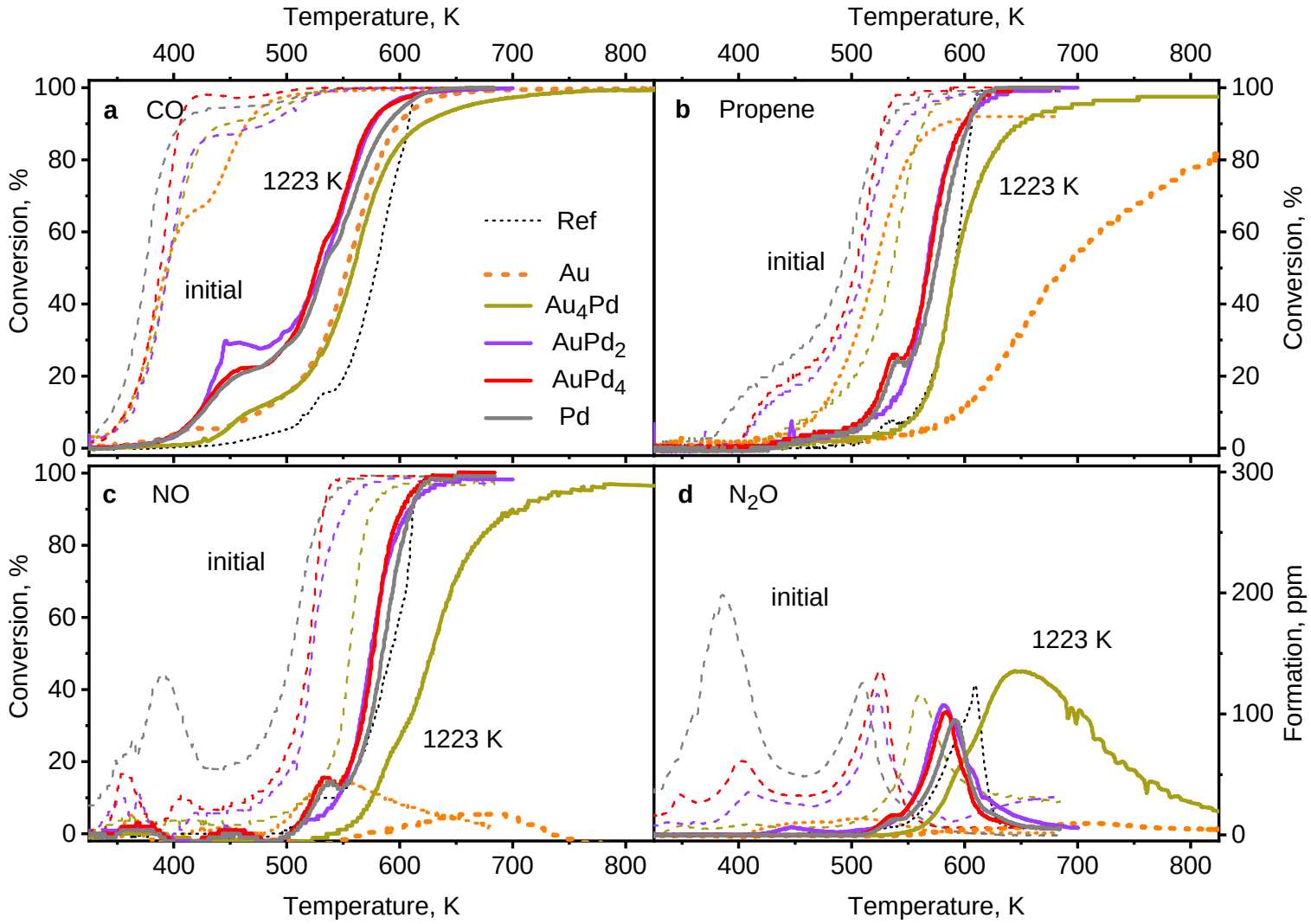

Figure 7 – Influence of ageing at 1223 K on the catalytic performance of LA-supported Pd, Au, and AuPd catalysts and of a commercial reference in the conversion of a TWC model feed; conversions of CO (a), of propene (b), of NO (c), N_2O formation (d).